Numerical Simulation of Nanoscale Flow:

A Molecular Dynamics Study of Drag

By

Tim Sirk

Thesis submitted to the faculty of the

Virginia Polytechnic Institute and State University

in partial fulfillment of the requirements for the degree of

Master of Science

in

Mechanical Engineering

Dr. Eugene Brown, Chairman
Mechanical Engineering

Dr. Mark Paul
Mechanical Engineering

Dr. Eugene Cliff
Aerospace Engineering

April 28, 2006
Blacksburg, VA

Keywords: Nano, Drag, Sphere, Biosensor
Copyright 2006, Tim Sirk

Numerical Simulation of Nanoscale Flow:

A Molecular Dynamics Study of Drag

By

Tim Sirk

(ABSTRACT)

The design of pathogen biosensors may soon incorporate beads having a nanoscale diameter, thus making the drag force on a nanoscale sphere an important engineering problem. Flows at this small of a scale begin to appear "grainy" and may not always behave as a continuous fluid. Molecular dynamics provides an approach to determine drag forces in those nanoscale flows which cannot be described with continuum (Navier-Stokes) theory.

This thesis uses a molecular dynamics approach to find the drag forces acting on a sphere and a wall under several different conditions. The results are compared with approximations from a Navier-Stokes treatment and found to be within an order of magnitude despite the uncertainties involved in both the atomic interactions of the molecular dynamics simulation and the appropriate boundary conditions in the Navier-Stokes solution.

Acknowledgements

I would like to thank the faculty of the Interdisciplinary Center for Applied Mathematics at Virginia Tech for the use of their SGI Origin 2000 as well as the staff of the Computational Physics & Fluid Dynamics Division of the Naval Research Laboratory (NRL) for the use of their SGI Origin 3200. A special thanks to Bill Sandberg for his insight and suggestions during my stay at NRL.

I would like to express my gratitude to Dr. Eugene Brown for his guidance during the course of this research. Our many conversations regarding thermodynamics and fluid dynamics have been very insightful. Dr. Eugene Cliff and Dr. Mark Paul have also been great resources and were kind of enough to serve as members of my committee. A special thanks to Dr. Zhigang Li for sharing his experiences modeling drag force with molecular dynamics.

A final thanks to my wife, Hanh Vu, for her support and newfound appreciation of atoms.

The first principle is that you must not fool yourself - and you are the easiest person to fool.

-Richard Feynman

Table of Contents

Table of Figures

Chapter 1: Introduction to Molecular Dynamics

1.1 Motivation

A renewed interest in detecting chemical and biological agents has encouraged researchers to improve old biosensor designs as well as develop new ones. Two microbead-type biosensors under development at the Chemistry Division of the Naval Research Laboratory are the Bead Array Counter (BARC) and Force Discrimination Biosensor (FDB). Downsizing these biosensor designs could be a major step forward in both sensitivity and analysis time with the added benefit of lab-on-a-chip technology.

A process within both biosensor designs involves removing a number of micron size beads from a fluid-filled channel using either magnetic or fluidic forces. In the future, it will be desirable to significantly shrink these beads for the sake of performance, perhaps down to the nanoscale level. The behavior of these nanobeads would enter a realm of physics not accessible to continuum fluid dynamics.

The behavior of nanobeads is important to performance, particularly when a bead moves near a channel wall. The biosensor is designed such that nanobeads either attach themselves directly to a channel wall or become tethered to the wall by DNA. For best performance, these designs require an understanding of the flow behavior around nanosize objects, especially spheres, near and at a channel wall. Gijs provides a more complete introduction to biosensors [Gijs, 2004].

1.2 Common Uses of Molecular Dynamics in Fluid Mechanics

Classical fluid mechanics assumes fluid motion is governed by the Navier-Stokes equations. This model has proven quite accurate since its conception and still remains the dominant model of fluid dynamics. However, recently some systems of interest have

become small enough to be modeled discretely on an atomic scale. In these situations, a purely continuum description of fluid motion is obviously inappropriate.

How a system is to be modeled usually begins by judging the length scale of the problem. Several important physical models with their corresponding length and time scales are shown below in Figure 1.1.

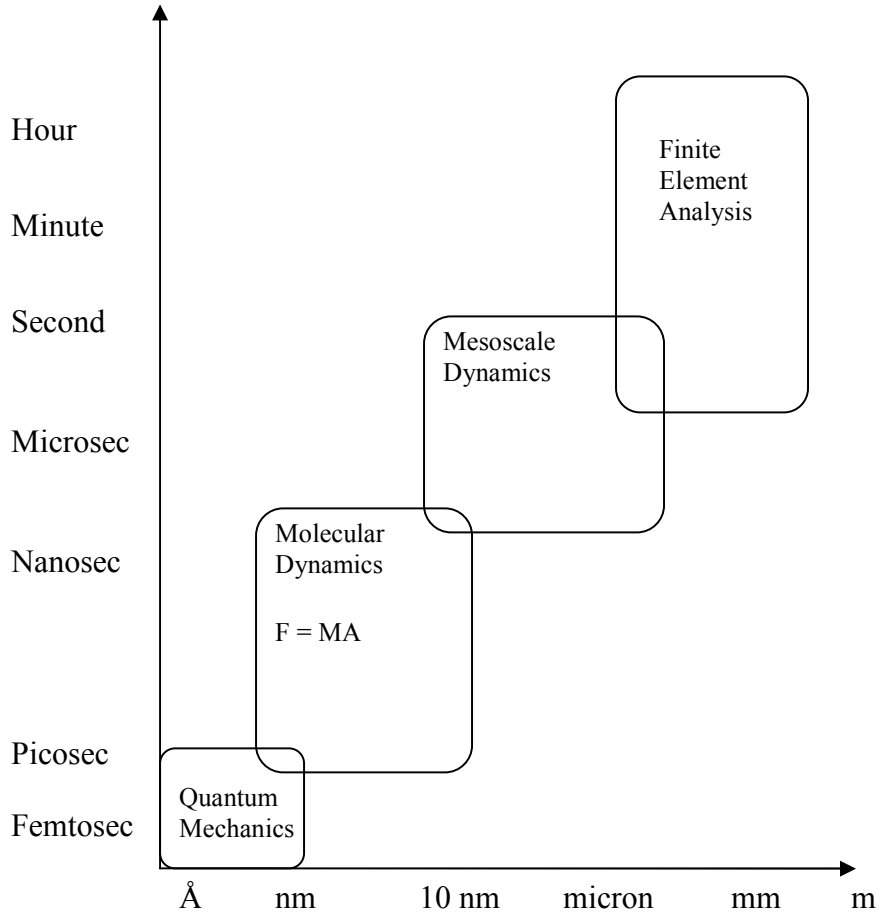

Figure 1.1. Modeling methods in discrete and continuum regimes.

Because the diameter an atom is comparable to a characteristic length of the problem's geometry, flow systems with dimensions of order 10^{-9}m are best treated as discrete collections of atoms rather than a continuous fluid. For example, the Navier-

Stokes solutions for Poiseuille flow are typically reliable down to a channel diameter of 10 molecular widths [Travis, 1997]. Beyond this limit other modeling methods must be used to describe the fluid motion.

Analytical solutions of multi-body problems are usually not practical for any discrete fluid of a significant volume. Statistical mechanics provides insight into a few cases with limiting behavior; however, computational methods are available that evaluate fluid behavior under many more conditions.

Notice in Figure 1.1 that molecular dynamics (MD) is sandwiched between the infinitesimal world of quantum mechanics and mesoscale dynamics. Many sciences are able to use a mesoscale model to bridge MD and continuum theory, such as nucleation modeling in material science. The mesoscale "bridge" serves to save time when the detailed results of MD are not needed; however, this approach is not always applicable. Fluids generally do not form mesoscale structures and jump directly from MD to continuum theory, provided that an acceptable MD model is known. Monte Carlo and Lattice Boltzmann methods (not shown) overlap both the upper domain of MD and the lower domain of continuum length scales, but obtaining information concerning the movement of individual atoms still requires an MD simulation.

Unlike Lattice Boltzmann and Monte Carlo, MD provides a complete description of fluid behavior by finding the trajectory of each atom or molecule as it moves within a fluid. Probabilistic input, such as velocity distribution functions, is not part of an MD model. Unfortunately, an MD approach is computationally expensive and the volume of fluid that can be modeled remains limited despite advances in computer power [Haile, 1997].

The time consuming process of generating detailed information about each atom in the fluid does provide MD with one striking advantage: A broad range of problems

may be solved in a conceptually straightforward way. As long as the appropriate interatomic forces can be calculated, any boundary conditions are completely modeled thus leaving only the number of atoms as the primary factor in deciding which problems may be solved.

MD simulation typically does not model forces directly from quantum mechanical effects, instead forming all quantum considerations into classical potential energy functions. The Lennard-Jones potential is perhaps the most famous of these, although many exist. Many potentials can accurately describe the behavior of only a few substances. For example, the Lennard-Jones 12-6 potential is known for its accurate description of argon gas [Haile, 1997].

Outside of its original use in the simulation of static, or "equilibrium" fluids, MD is often used in simulations of fluids under a net external force. These "nonequilibrium" processes involve motion caused by sources other than thermal energy, such as pressure driven flow in a nano-dimensional channel. Simulation employing these processes is described as nonequilibrium molecular dynamics (NEMD) [Haile, 1997].

1.3 Foundations of Molecular Dynamics

Some results of statistical mechanics are needed to determine physical properties of the fluid during the simulation. In this work, as in the majority of other MD fluid simulations, a closed system with a constant number of atoms, constant volume, and constant energy is used. All of the possible physical states of a system with this combination of fixed properties are known as the microcanonical ensemble (NVE).

The temperature of a fluid is evaluated from statistical mechanics (from the microcanonical ensemble) as

$$T(t) = \frac{KE(t)}{3/2\, Nk_B} \tag{1.1}$$

where N is the number of particles, k_B is Boltzmann's constant and KE is the kinetic energy of the system [Haile, 1997]. Kinetic energy is determined as

$$KE\ (t) = \frac{1}{2}\sum_i m_i \left[v_i(t)\right]^2 \tag{1.2}$$

where m_i and v_i are the mass and velocity of each atom, respectively [Haile, 1997]. Atomic fluids are not permitted to store kinetic energy in the rotation of individual atoms. Kinetic energy and temperature are two properties that, along with the total energy, are usually tracked during an MD simulation. Other common thermodynamic properties, such as pressure, may also be tracked.

Any instantaneous system property can be followed during the simulation and used later to extract the macroscopic state of the system. Measurement of a physical property in the simulation is simply obtained as an average of the instantaneous values assumed by that quantity over a given time. The time average of a property A is equivalent to the microcanonical ensemble average of the instantaneous property and is defined as

$$\langle A \rangle_{\mathrm{NVE}} = \frac{1}{N_T} \sum_{t=1}^{N_T} A(\Gamma(t)) \tag{1.3}$$

where N_T is the total number of timesteps, $\Gamma(t)$ is the phase space coordinates of the system and A is the instantaneous property. The equivalence of the ensemble average and time average is known as the *ergodic hypothesis*. Taking advantage of the ergodic hypothesis allows MD simulations to avoid the difficult task of determining thermodynamic properties (ensemble averages) directly. See the appendix for a more complete explanation. Useful trends can be extracted from the time averaged properties, such as a phase diagram [Haile, 1997].

The numerical method used by MD is explored in the remainder of this chapter. In a general sense, MD is a computer simulation technique that follows the temporal evolution of interacting atoms by integrating the governing equations of motion. An MD simulation generates information at the microscopic level, including atomic positions and velocities. MD is a deterministic technique - given initial positions and velocities, the time evolution of the system is completely determined.

An MD algorithm simply provides the means to solve equations of motion numerically. The laws of classical mechanics, specifically Newton's 2nd law, govern particle behavior in a classical MD simulation. Newton's 2nd law is applied to each atom in an *N*-atom system where the atoms are allowed to interact. Forces and velocities are computed for a position, new positions are found and the system is moved one step forward in time. This cycle repeats throughout the simulation until terminated by the user.

This thesis determines the force acting between atoms from a classical, two-body potential that is only a function of the position of the two atoms. All quantum mechanical effects are assumed to be included within this classical potential. Some substances (not modeled in this thesis) require a more sophisticated approach and may need potentials that are a function of many variables such as local density, angle or temperature. Further, the modeling of a complex interaction may need to bypass the use of a potential altogether – instead, a simplified Schrödinger equation is solved.

1.4 The Scope of Molecular Dynamics

Like any methodology, MD is most at home within a set of limitations, outside of which, the results are not applicable. Two important limitations of MD are (1) the use of

classical forces to model quantum mechanics, i.e., the accuracy of potential functions, and (2) demands on computational power.

1.4.1 Classical Forces

The use of Newton's laws to move atoms is not entirely obvious since systems at the atomistic level experience forces governed by quantum mechanics rather than classical laws. Schrödinger's equation alone may govern motion at the atomic scale but a classical approximation can be very accurate in many engineering situations. The de Broglie thermal wavelength can test the approximation of using classical forces and is defined as

$$\Lambda = \sqrt{\frac{2\pi\hbar^2}{Mk_BT}} \tag{1.4}$$

where M is the atomic mass and T the temperature. The approximation is justified if $\Lambda << a$, where a is the mean nearest neighbor separation.

Classical forces are a poor approximation for low mass elements such as H and He. Notice the inverse √T dependence as well: any system at very low temperature is dominated by quantum effects. Results from MD simulation must be interpreted carefully in these situations. Further, a classical potential should not be used for those interactions that form covalent bonds or otherwise share electrons easily since these interactions are dominated by non-Newtonian physics [Hansen, 1986].

1.4.2 Computational Power

MD simulation can be performed on systems that contain thousands, hundreds of thousands or even millions of atoms, depending on the application [Haile, 1997]. Biomolecular systems are typically small because elaborate potentials are usually required, however atomic liquids and solids modeled with only the Lennard-Jones potential can be built with many more atoms. Generally, the ability to model a large

system allows a greater variety of problems to be solved, since the size of the MD simulation box should not be $O(1)$ with characteristic lengths of interest. The two factors of time and size always limit MD simulation and often one must be compromised for the other.

Simulation times range from a few picoseconds to hundreds of nanoseconds, although several nanoseconds could be considered typical for NEMD simulation of liquids on a moderately powerful parallel computer. At any rate, the timescale associated with MD is much less than that of some physical phenomenon. A simulation has an acceptable duration when the simulated time is much longer than the relaxation time of the quantities being investigated; however, different properties have different relaxation times [Haile, 1997]. In particular, systems tend to become sluggish near phase transitions and it is possible that the relaxation time of a property is much larger than can be achieved by simulation. Boiling of water at a temperature slightly higher than 100 ºC (1.0 atm) is such a case [Zahn, 2004].

1.5 Potential Energy Models

In classical MD, forces are obtained as the gradient of a potential energy function; the behavior of every atom in the simulation then depends on the choice of the potential function(s). Simple potentials are both translationally and rotationally invariant and are a function of the relative positions of the atoms in the simulation box. By allowing the potential to only depend on position, it is inherently assumed that electrons adjust to new atomic positions much faster than the motion of the nuclei (the Born-Oppenheimer assumption) [Born, 1927]. In fluid simulations, many researchers use potentials with a two-body interaction because of the added complexity of an N-body interaction, although many-body potentials are commonly used, particularly in the simulation of metals and condensed matter.

Energy conservation in a system governed by two-body interactions can be examined at equilibrium by monitoring the sum of the kinetic energy from Eq. 1.2 and the potential energy of the system. For a two-body potential, the potential energy φ of the system is the sum of all pairwise interactions:

$$V(r_1, ..., r_N) = \sum_i \sum_{j>i} \phi(|r_i - r_j|) \tag{1.5}$$

Where the j>i condition of the second sum allows each atom pair to be considered only once.

Many potential models exist to model a variety of atomic interactions; however, the two-body Lennard-Jones 12-6 potential is perhaps the most basic and widely used in molecular dynamics. For a single pair of atoms, it is defined as

$$\phi_{LJ}(r) = 4\varepsilon\left[\left(\frac{\sigma}{r}\right)^{12} - \left(\frac{\sigma}{r}\right)^{6}\right] \tag{1.6}$$

The exponentials 6 and 12 are chosen empirically. The interatomic force is found as the 1st derivative,

$$F_{LJ} = -24\varepsilon\left[2\left(\frac{\sigma^{12}}{r^{13}}\right) - \left(\frac{\sigma^{6}}{r^{7}}\right)\right] \tag{1.7}$$

Defining a positive force to be repulsive, the potential has an attractive exterior with a repulsive core. The force is strongly repulsive force at short distance, passes through zero at 1.122σ and extends to infinity with a long, attractive tail.

The 12-6 LJ potential has only two parameters, ε and σ, that are properties of the substance. Other variations of the LJ potential may use different exponents [Haile, 1997]. A plot of the12-6 LJ potential is shown in Figure 1.2.

The $1/r^{12}$ term of Eq. 1.6, dominates at short distance and models the repulsion between nearby atoms. Physically, the Pauli exclusion principle prevents two fermions (electrons belong to this class of elementary particles) from occupying the same quantum

state, thus the repulsive force is caused by the overlapping electron clouds of neighboring atoms [Ohanian, 1995].

The $1/r^6$ term produces the attractive part of the potential. Van der Waals forces are responsible for producing this induced dipole-dipole attraction. It is a comparatively weak attractive force, but still dominates interactions in atomic elements with a full outer electron shell such as argon. The LJ potential does in fact model argon and krypton, another noble gas, well at moderate temperatures.

The contribution of both terms is shown below in Figure 1.2.

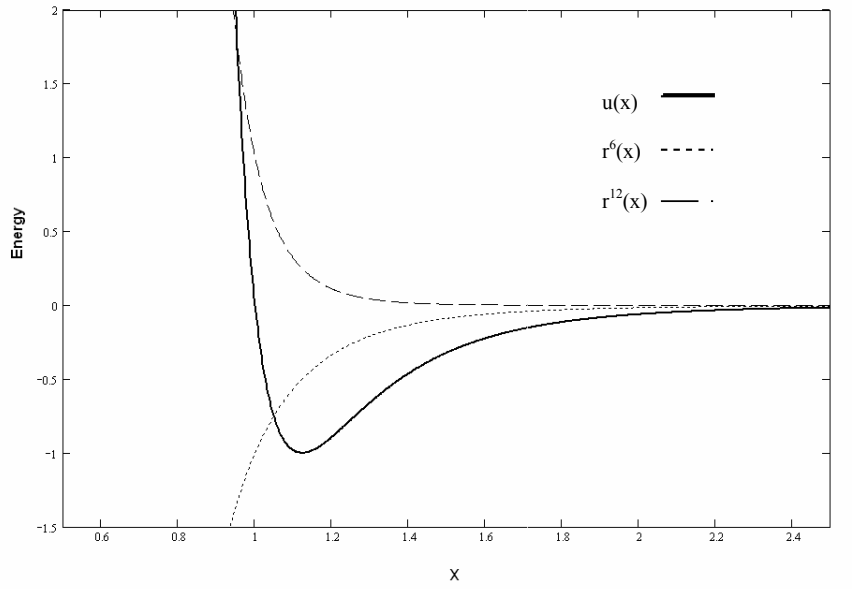

Figure 1.2. Components of the Lennard-Jones potential. The minimum energy is located at $x = 2^{1/6}\sigma = 1.12\sigma$.

Despite its inability to predict all interatomic forces, the LJ potential is often still used as a starting point because of its computational efficiency when compared with more accurate potentials. In fact, many authors apply the LJ potential to systems when the focus is to only show qualitative behavior, such as the film growth of metals [Guan, 1996]. The LJ potential has become so instructive that it is often thought of as the generic potential in MD.

1.6 Potential Energy Truncation and Long-Range Corrections

The infinitely long attractive tail of the Lennard-Jones potential can create practical problems. By imagining an atom interacting with other atoms at a distance r, it is seen that as r increases linearly then, for a fixed density, the number of atoms scales with r^3 (volume). This creates a serious problem of computation power if the system is to be simulated for any worthwhile amount of time. One effective solution is to disregard interactions outside of a radius R_c where the attractive tail contributes very little to the system's behavior. However, truncating the potential creates a problem with energy conservation. When one atom moves within the "cutoff" radius of another, the system undergoes a small but finite jump in potential energy and alternatively, a loss when an atom leaves the cutoff radius. This leads to an energy fluctuation of the system, even while in the microcanonical ensemble. A possible solution is to "shift" the potential function so that the potential energy goes smoothly to zero at the cutoff radius. The shifted LJ potential is defined as

$$F_s(r) = \begin{cases} -\frac{du}{dr} + \Delta F & r \le R_c \\ 0 & r > R_c \end{cases} \tag{1.8}$$

where F_s is the sum of the force resulting from the LJ potential and a correcting force ΔF. This approach creates another problem by changing the potential energy for $R < R_c$ [Haile, 1997]. Rather than using this less accurate LJ potential, the impact of the truncated potential in fluid can be lessened by extending the cutoff radius or, as in most literature, ignoring the small amount of noise in the potential energy [Haile, 1997]. The LJ 12-6 potential with a cutoff radius of either 2.5σ or 3.2σ is widespread in MD literature, with 2.5σ being used in this work.

1.7 Periodic boundary conditions

One important feature of micro- and nano- scale systems is a large surface to volume ratio. An MD simulation is typically limited to a simulation "box" of a few tens of nanometers in dimension. There are a great number of atoms at or near the surface of the simulation box, making a bulk fluid difficult to model if solid walls are used to contain the atoms. Alternatively, the kinetic energy of the fluid causes the atoms to push out of the simulation box if no walls are used.

A large volume of atoms (requiring a lengthy runtime) could be implemented, but a more practical way to eliminate surface effects is the use of periodic boundary conditions (PBC). PBC in Cartesian coordinates specify that a dimension of space has a closed geometry[I]. This has two important consequences: (1) Atoms leaving one face of the simulation box immediately emerge from the opposing face with the same momentum and (2) atoms within the cutoff distance of a simulation box boundary interact with atoms near the opposing face of the simulation box.

Interactions can now penetrate box boundaries and eliminate surface effects from the system. The position of the box boundaries has no effect on the behavior being observed; however, it is now unclear which distance the two-body potential will use for a displacement. The *minimum image criterion* defines a way to determine where two atoms are actually located within the simulation box. It states that the two-body potential must always compute forces using the closest distance (rather the farthest) to another atom [Haile, 1997].

An alternative explanation of periodic boundary conditions is shown below in Figure 1.3. A continuously updated copy of the simulation box is joined to each face of the actual simulation box. An atom within the cut-off radius of a boundary is affected by

[I] The similarity of the system with a closed, non-Euclidean geometry is limited since the angles of a triangle in the simulation box still add to 180˚.

other atoms in the boundary of the neighboring box, which are identical to atoms on the opposite boundary of the real simulation box. Although this 'replica' approach to describing PBC is conceptually more complicated than a simple closed geometry, the necessary programming details are more apparent.

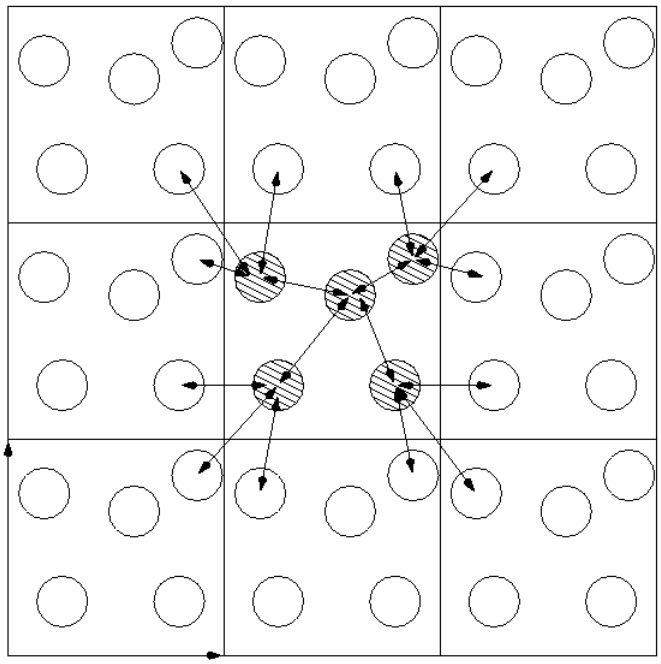

Figure 1.3. Periodic Boundary Conditions [Veytsman, 1997]. Atoms interact across the boundaries of the simulation box. ***Illustrated under "Fair Use" copyright guidelines.***

1.8 Time integration algorithms

The heart of a molecular dynamics program is the time integration algorithm. This finite difference algorithm integrates the equations of motion for the interacting atoms, computes forces and tracks the position of atoms in time.

Several time integration algorithms are common, with the Verlet and the predictor-corrector being the two most popular classes of MD algorithms. Each has advantages but all are approximate and have some common sources of error. A Taylor expansion is used in the derivation of both these methods with the contributions of higher

order terms being neglected. Also, the precision implemented in the particular code will ultimately cause round off errors. Both of these errors can be minimized by decreasing the timestep and increasing the numerical precision set aside by the program [Haile, 1997].

Predictor-corrector methods advance the simulation in time by predicting an acceleration with a Taylor expansion then later correcting the acceleration when the force is formally evaluated from the gradient of the potential. These methods require eight arrays of size 3N, which is five more than required by the popular Verlet schemes. A specific interpretation is the Gear predictor-corrector, which is fifth order accurate and can use a longer timestep than Verlet methods, thus making it both more accurate and more stable [Haile, 1997].

The Verlet algorithm is a good compromise between accuracy and performance. The MD algorithm in this thesis uses a Verlet variant known as the velocity Verlet algorithm which explicitly includes the velocity in the algorithm and is therefore self starting when provided positions and velocities. Although it is mathematically identical to the standard Verlet scheme, the kinetic energy in the Verlet velocity algorithm may be computed immediately rather than requiring an extra step to compute atomic velocities [Haile, 1997].

Simulations involving external inputs such as external forces or artificially fixed velocities add energy to the system and cause an increase in temperature. In this type of simulation, it is often desirable to hold the system or a body within a system at a given temperature. One convenient way of maintaining a fluid at a constant temperature is modifying the equations of motion in the time integration algorithm. Velocities in the region to be thermostated are rescaled upwards or downwards such that the desired temperature is maintained. Actual velocities V_{act} are replaced with V_{set}:

$$V_{set} = V_{act}\sqrt{\frac{T_{set}}{T_{act}}} \tag{1.9}$$

where T_{set} is the desired temperature and T_{act} is the current temperature [Haile, 1997]. At this point, Newton's laws are no longer being used; an artificial velocity correction proportional to $T(t)^{-1/2}$ causes the actual velocity to converge to the velocity needed for the set temperature. Although the thermodynamic properties of this system are identical to that of a closed system, caution should be exercised if the trajectories of individual atoms are followed. This method of temperature control will be adopted for this thesis, but it is only one of several well known "thermostats".

Chapter 2: Literature Review

2.1 *Historical Background*

A brief discussion of MD history and relevant past works is presented here to properly position this research within the context of MD literature.

The principles of MD were well understood long ago, but without a computer little could be accomplished. Not until the 1950s could MD even yield results for simple, idealistic systems with a small number of particles. As the computer evolved, important contributions were made in many fields ranging from crystalline defects in solids to nanofluidics.

Researchers using MD find themselves in a situation opposite that of their colleagues involved in experimental work; investigation at an ultra small scale turns out to be *easier* than at the macro scale. It should be no surprise that atomic fluids were a natural first application since an arbitrary number of atoms can form the volume of fluid to be analyzed. Fluids, particularly liquids and rarified gases, still remain an open subject in MD.

The first research reporting a molecular dynamics simulation was published by Alder and Wainwright [Alder, 1957]. The work investigated the phase diagram of a hard sphere system, particularly the solid and liquid regions. In a hard sphere system, particles interact via instantaneous collisions and travel freely between collisions. Important insights concerning the behavior of simple liquid simulations emerged from their studies. Fluid properties were becoming a specialty of MD immediately after its conception, but the sluggish vacuum computers of the 1950s were only suited for very small systems with simple potentials. The above calculations were performed on a 25 ft x 50 ft UNIVAC vacuum tube computer operating at 2.25 MHz.

The next major advance was in 1964, when Aneesur Rahman carried out the first simulation using a realistic potential for liquid argon [Rahman, 1964]. Rahman is well known as a founder of modern molecular dynamics and made important breakthroughs concerning the properties of liquid argon and the Lennard-Jones potential. Although Rahman's work began as a method of modeling neutron scattering, it contained many of the important features used in nanofluidic MD simulation today. The truncated LJ potential, periodic boundary conditions and modern parameters for liquid argon were all included. Rahman realized that liquid argon would be an ideal substance for simulation because of its unique ability to be modeled by the LJ potential.

The algorithms used in MD were also improving at a fast rate. In 1967, Loup Verlet introduced the bookkeeping scheme known as *Verlet neighbor list*. This bookkeeping device kept a list of neighbor atoms within each atom's cutoff radius plus an additional length know as *skin thickness*. When an atom traveled outside the skin thickness, the list was rebuilt so that an updated list of nearby atoms was always available. The program no longer needed to check the coordinate of every atom to determine which atoms were within the radius of the cutoff potential. Using the neighbor list technique, only the distance to nearby atoms must be calculated at every timestep. Neighbor lists are still considered a staple of MD code today. The celebrated Verlet form of the time integration algorithm was also introduced [Verlet, 1967]. Verlet was able to apply his new technique to match an actual phase diagram of liquid argon with one calculated from directly from MD simulation. His system contained only 864 atoms. Like Verlet, the majority of early researchers in this field derived transport properties from equilibrium molecular dynamics, with viscosity being the most common subject. NEMD simulation was later used to determine many of these same transport properties.

The obvious extension of NEMD was the modeling of classic Navier-Stokes solutions such as Poiseuille and Couette flow, but a realistic investigation would only be possible using the computer power of the 1980s. Publications related to boundary conditions on a solid surface, Poiseuille flow, Stokes drag and other pieces of literature relevant to this work are discussed below.

2.2 Poiseuille Flow

The modeling of Poiseuille flow accelerated in the late 1980s and 1990s. Koplik et al. began an important line of research in the 1988, with their study of Poiseuille flow and the no slip boundary condition [Koplik, 1988]. Basic properties of Poiseuille flow were first established from a microscopic level and compared with those resulting from a continuum assumption.

For a low Reynolds number flow though a channel, the well known parabolic velocity profile was observed. This allowed the fluid's viscosity to be determined by matching a curve fit of the velocity profile to a Poiseuille flow solution. The no slip condition was observed to arise naturally from the wall-fluid interaction.

In another work [Koplik, 1989], a continuum solution containing a divergence in the shear stress at a moving contact line is resolved by MD simulation. A moving contact line forms when two immiscible fluids meet on a translating solid surface. Applying the no slip condition at the solid surface leads to an infinite stress at the contact line. The situation may be resolved analytically by relaxing the no slip condition near the contact line. Koplik et al. showed the physical reasoning behind this assumption through a molecular dynamics simulation of Poiseuille flow involving the two fluids. The no slip condition is shown to fail near the contact line but holds elsewhere along the surface. Using MD to resolve divergences in continuum fluid mechanics would become a common theme in the later work of this and other authors.

In the same publication [Koplik, 1989], Koplik also detailed the fluid's behavior closely, specifically near the wall. Fluid atoms were observed to form discrete, well-defined layers near a wall of FCC (faced centered cubic) structure. There layers were represented as sharp density oscillations that decreased in positions toward the center of the channel. Further, fluid atoms near the FCC structured wall were most likely to be found in a similar FCC arrangement. This study was not the first to observe organized fluid structure near a surface, but certainly helped the formation of atomic layers near a surface to become a well known observation in the nanofluidics community.

Koplik et al. also document velocity slip at low fluid densities. In a sequence of densities from 0.8 to 0.08 N/σ^3 (at a fixed temperature), a smooth transition to slip is observed in Poiseuille flow. Continuum descriptions of velocity slip in rarified gas support this observation.

The MD study of polyatomic fluids began with Rahman et al. in the simulation of liquid water [Rahman, 1974]. More complex fluids have been modeled since and these have been found to produce properties near to that of a continuum fluid in large enough systems. Exceptions to the behavior predicted by a continuum description do occur when a channel is narrow enough to cause a failure of the Navier-Stokes equations. This problem is addressed by Travis et al. [1997]. Channels having a width somewhat less than 10 atomic diameters are seen to diverge from the parabolic velocity profile predicted by Navier-Stokes calculations.

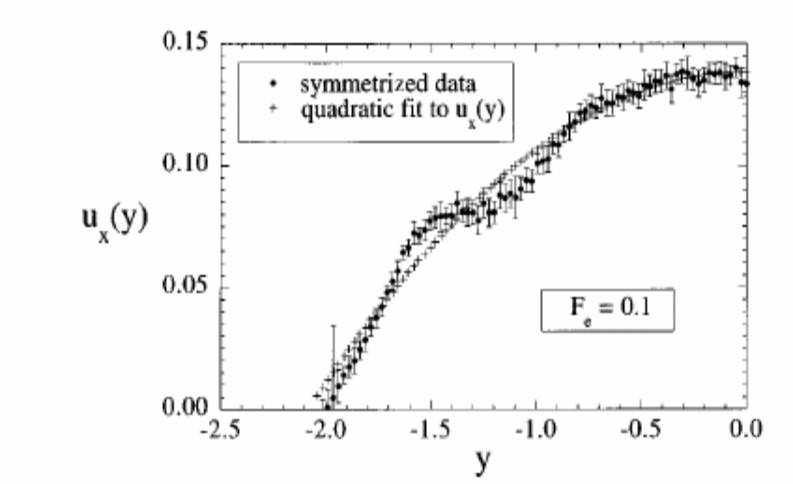

Figure 2.1 [Travis, 1997]. The velocity profile of a small channel of width 5.1 atomic diameters in 2D Poiseuille flow. ***Illustrated under "Fair Use" copyright guidelines.***

As seen in Figure 2.1, a "stair step" can be formed in the velocity profile of nano-scale channels. A quadratic fit represents the parabolic profile expected from a Navier-Stokes solution. The stair step profile becomes much less pronounced as the channel width increases as seen in Figure 2.2. However, a careful inspection of Figure 2.2 near y = -4.0 still reveals some faint remnants of the failure of the Navier-Stokes equations.

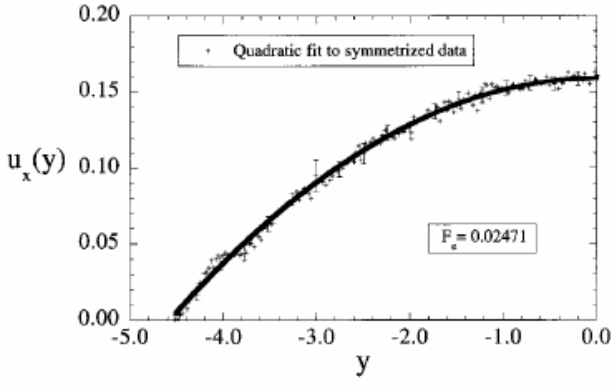

Figure 2.2 [Travis, 1997]. The velocity profile of channel of width 10.2 atomic diameters. ***Illustrated under "Fair Use" copyright guidelines.***

2.3 Drag Force and Stokes Law

The 1980s held several important accomplishments related to external flow, including the exploration of eddies by D.C. Rapaport et al. [1986]. This work examined the formation of eddies using 100,000 atoms with a simple, repulsive potential. It was the first MD study of a large number of particles flowing around an obstacle.

Rapaport et al. simulated a two-dimensional flow past a circular obstacle with the use of periodic boundary conditions. Fluid collisions with the obstacle were modeled as both having a specular reflection, implying a slip boundary, and as having random reflection, resulting in a no-slip condition. The choice of boundary condition was found not to affect the results. At sufficiently large Reynolds numbers, the flow field demonstrated characteristics of continuum fluids such as eddies, eddy separation and an oscillating wake. The authors were able to directly compare their results to extensive photographic documentation and continuum numerical solutions of eddy formation. The Strouhal number, a nondimensional number associated with wake oscillation, of the simulation was found to compare well with continuum data. D.C. Rapaport developed one of the first parallel MD codes, which he used on four processors for this simulation.

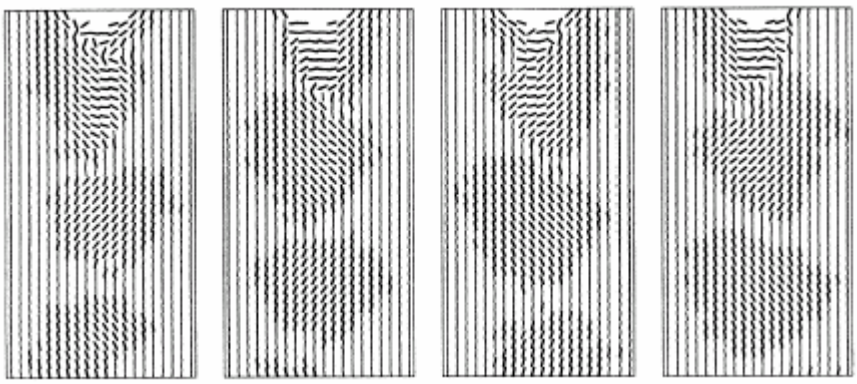

Figure 2.3. Examples of wake oscillations from the back of a disk [Rapaport, 1986].

Illustrated under "Fair Use" copyright guidelines.

Next, an important work by Koplik et al. detailed the drag force associated with an atomic sphere while undergoing either translation or rotation in an atomic fluid [Koplik, 1996]. The modeling of the sphere's translation served as both an inspiration and starting point for this thesis. In Chapter 5, the drag force found in this reference is used to confirm the initial modeling performed in this thesis.

The authors found several similarities with continuum results. In particular, Stokes' drag [Stokes, 1851] was found to match the MD solution closely. Stokes law states that the drag force on a sphere moving at low Reynolds number through an infinite, viscous fluid can be approximated as

$$F = 6\pi\mu bU \tag{2.1}$$

where μ is the dynamic viscosity, b is the sphere radius and U is velocity of the sphere. All of these parameters are known, so the continuum result is easily obtained and compared with the drag force found from MD simulation. Rather than comparing drag directly, the authors compute the sphere radius b and compare with the nominal sphere radius. Agreement of the computed and nominal radii is found to be good at different velocities and sphere sizes. The authors are also able to use MD to resolve two cases of an unphysical divergence in solutions of the Navier-Stokes equations for a sphere near a wall. Both divergences were rooted in the use of the no-slip condition.

As with previous studies, fluid density was observed to be heterogeneous near the walls. The spontaneous layering of fluid is best documented by Barrat et al. [1994]. Six visible, organized layers were observed as shown in Figure 2.4 below.

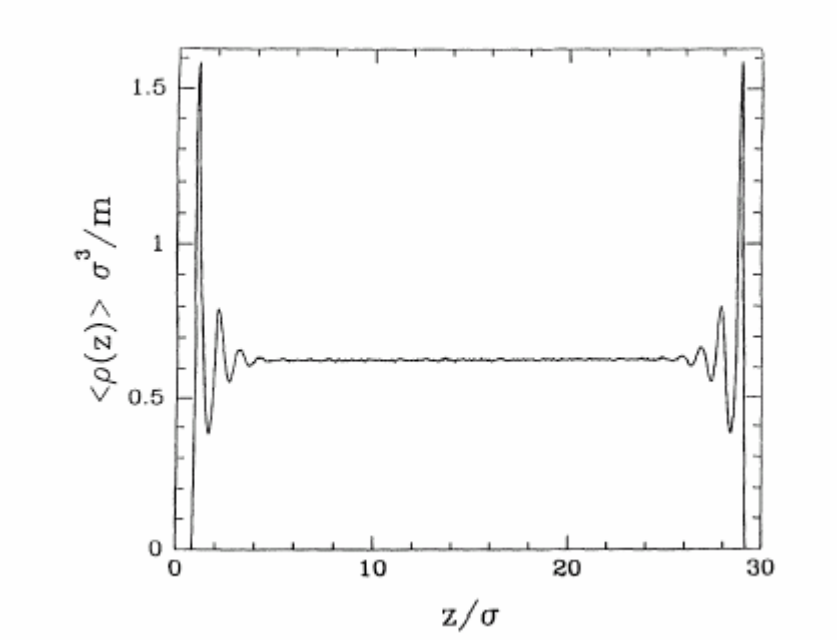

Figure 2.4. Density gradients across a channel bound by molecular walls [Barrat, 1994].

Illustrated under "Fair Use" copyright guidelines.

2.4 Wall Models

Koplik et al. employed a sphere that was held in shape by the large mass of the individual atoms. Many walls in MD fluid simulations are modeled in a similar way [Sun, 1992; Koplik, 1988, 1989, 1996] rather than employing more elaborate schemes that require computationally expensive nonlinear springs [Travis, 1997] or other modified bonds.

Sun and Ebner developed several wall models in the early 1990s and studied the fluid-wall interface [Sun, 1992]. One interesting model combines a continuous 10-6 LJ potential, the "heavy" type wall atoms mentioned above and a bonding potential between the wall atoms. A uniform (non-atomic) wall having a continuous 10-6 LJ potential was covered with six layers of atoms which were both heavier and had a more attractive potential than the fluid atoms. This composite approach addressed some of the problems with earlier wall models.

Ideally, walls should be made of a large number of layers connected by realistic bonds; however, the amount of computational power available for simulating the fluid would be reduced. Bonding between atoms in a solid, such as a wall, also allows heat to be transferred in a realistic fashion at the expense of computation time. More wall layers are required to maintain the stability of a structure connected by bonds than a structure with atoms artificially held in place by some computational trick, such as giving the atoms a large mass.

Molecular structure within the wall is important since a few layers of fluid molecules tend to arrange themselves over the lattice sites of the wall; however, solid continuous walls are not without benefit. A single potential can be defined for an entire continuous wall, effectively making one large particle that replaces thousands of individual wall atoms. The wall of Sun and Ebner [Sun, 1992] creatively combine the advantages of both by using a molecular wall with a solid backing.

Later in 1990s, Koplik et al. led a more in depth investigation of the properties of molecular walls [Koplik, 1998]. They found that if the precise structure of the molecular wall is not important to the fluid behavior or, if behavior near the wall is not of interest, a "thermal" wall could then be substituted for a more complex atomic wall. It was found that walls can be stochastically treated as smooth surfaces that reflect fluid in a random direction with a magnitude related to the wall temperature. This significant work also clarified the mathematics of thermal walls and illustrated pitfalls in their application.

Thermal walls are much easier to implement than a full atomic description; however the model conceals some of the properties of a real atomic wall and is not widely used in NEMD.

2.5 Comprehensive References

Several useful texts were published in the 1990s that helped make MD accessible to those outside of the field. Haile developed a text [Haile, 1997] which included general techniques for solid and fluid systems that use hard sphere or LJ potentials. The book contained basic considerations for MD simulation and developed examples using FORTRAN code. This text still serves as an alterative for researchers not familiar with the C language used in an earlier text by Rapaport [1995].

Although both books are similar, Rapaport's book is the more practical for those interested in creating a custom code. Rapaport developed the basic framework of an MD program in a generic style of C code. In many ways, his text was also intended to be a "cookbook" of sorts for MD calculations, as was further emphasized in the 2nd edition published in 2004 [Rapaport, 2004].

Chapter 3: LAMMPS and Visualization Software

3.1 LAMMPS – Large Atomic Molecular Massively Parallel Simulator

LAMMPS is an open source, classical molecular dynamics code developed by Sandia National Laboratories. It is a C++ code capable of modeling atomic, polyatomic, biological, metallic or granular molecules using a variety of force fields and boundary conditions. Biomolecular systems requiring detailed modeling are a common use of LAMMPS simulation, thus the full potential of LAMMPS is not required for this work. Only a single potential, a time integration scheme, a simple thermostat and some basic preprocessing functions are needed.

Although LAMMPS runs efficiently on single processor workstations, it is designed for parallel applications. The maximum number of atoms that can be modeled in a simulation is dependent on computational power. In most atomic systems, the time required for computing scales linearly with the number of atoms in the system. The same linear scaling does not hold for the number of processors and limitations occur when any code runs in parallel on a multiprocessor machine. The overhead associated with communicating between processors becomes important and, given enough processors, will eventually dominate the computational time. A maximum of only 16 processors was used at any time in this work, meaning that most of the runtime is spent on molecular dynamics rather than processor communication.

While running in parallel, spatial decomposition techniques are used to partition the simulation box into three dimensional blocks which are divided among the processors. Processors communicate and store 'ghost' atoms, i.e., information about other atoms bordering the processor's assigned region of space. Other MD codes such as NAMD and NWCHEM also use spatial-decomposition approaches, however, the popular

codes CHARMM and AMBER use atom-decomposition methods for parallel operation. Plimpton provides an explanation of the specific time integration method used by LAMMPS [Plimpton, 1995].

Most of the LAMMPS runtime was logged by this author on a Silicon Graphics Origin 2000 at the Interdisciplinary Center for Applied Mathematics at Virginia Tech and an Origin 3200 at the Laboratory for Computational Physics & Fluid Dynamics at the Naval Research Laboratory. LAMMPS was also executed on the author's single processor PC after some minor programming updates to the source code. This was helpful in developing trial input scripts and troubleshooting small problems. Although functions within LAMMPS are designed for easy modification, the size of the code (35k lines) necessitates a good working knowledge of C++ to make significant changes.

3.2 LAMMPS Operation

As an input, LAMMPS requires a list of initial atomic coordinates and molecular topology information such as mass and force field coefficients for each atom. This information can be either entered at the LAMMPS input script or generated by a custom code which is called when LAMMPS reads the input script. In either method, a simulation box is defined and filled with atoms whose positions and properties are determined by the user. Thermodynamic properties are controlled by defining an ensemble and/or holding some properties constant. Microscopic mechanical characteristics such as velocity and momentum can be explicitly assigned to individual or groups of atoms.

Since the number or position of atoms within the LAMMPS simulation box is not restricted in any way, an ensemble of atoms may be produced in any phase. Care must be taken to assure that the fluid's properties yield the desired location on the phase diagram.

Once the system constraints are set, LAMMPS updates the system by the Verlet velocity integration scheme (see Section 1.8) over a predetermined number of timesteps. Integration is prematurely stopped if values stored in the program, such as a thermodynamic property, become unphysically large.

3.3 LAMMPS Pre- and Postprocessing

Several features are available within LAMMPS that automatically generate lattices and simple geometric shapes. A built-in preprocessor can produce sets of atom coordinates that correspond to different three-dimensional shapes. The LAMMPS preprocessor takes user input for the specific shape and assigns the required atomic coordinates to a text file. Both the wall and sphere of this thesis were generated with this preprocessor. More complex geometries can be created by bypassing the default preprocessor and inputting atomic coordinates via a text file; however, any geometric figure must always built from a collection of individual atoms which are positioned by the user.

Caution must be exercised as the atoms are being positioned. Any two atoms placed unnaturally close together can produce a near infinite repulsive force, which leads to a large temperature on the following timestep. The unexpectedly large force originates from the steep slope of the LJ potential near R=0 and is completely avoidable by a proper choice of atomic spacing. Despite its simplicity, this is a common problem. Each atomic position is defined by an algorithm that writes Cartesian coordinates to a text file, thereby assuming atoms to exist only as points. The algorithm is chosen to space these points properly but exceptions can occur near boundaries of two geometric regions or on the border of the simulation box when periodic boundary conditions are applied.

Most commonly, an atom located on one plane of the simulation box is accidentally imposed over another atom on the opposite side by periodic boundary

conditions. The proximity of the two atoms produces a large temperature that crashes the program. Locating the offending atom(s) is not always trivial and the details of the input script can become important in resolving these conflicts.

No postprocessing operations are available with LAMMPS. Postprocessing duties are handled by a multi-functional code created by the author. This code allows the user to find the instantaneous drag force, average net drag force and atomic velocity distribution over a range of timesteps. These quantities and related data are printed to a text file so that further analysis can be performed with a spreadsheet program.

3.4 Visual Molecular Dynamics

Despite being one of the simplest forms of data analysis, having a visual output is vitally important in molecular dynamics. During the research documented in this thesis, the system exhibited unusual flow patterns, freezing, loss of atoms and other unexpected phenomena. Each time the unusual event could be immediately observed from the visualization and traced back to a minor mistake in the input script. Subtle mistakes, especially syntax problems, are easily overlooked in the input script but rarely go unnoticed in the visualization.

Although several good visualization codes exist, Visual Molecular Dynamics (VMD) is used throughout this work. VMD is specifically designed for visualizing biological and molecular systems and, like LAMMPS, it is more than adequately equipped to handle a flowing atomic fluid. The Theoretical Biophysics Group at the University of Illinois at Champaign developed this open source code for public use [Humphrey, 1996].

VMD provides a way of animating an otherwise abstract collection of data. LAMMPS provides the coordinates for all the atoms of the simulation to VMD over a series of timesteps in the form of a properly-formatted text file. Because the atoms are

represented by only a set of coordinates, a common approach to visualizing an atom is to assign a radius from the coordinate and fill the volume inside this radius with a solid color. Despite its ad hoc nature, the sphere has a counterpart in the repulsive core of the LJ potential, or in a more physical sense, the electron cloud of a real atom.

VMD has a large variety of color schemes and visualization styles. The user may choose to work with the excellent VMD graphical interface or use the command prompt. A screenshot is shown below in Figure 3.1.

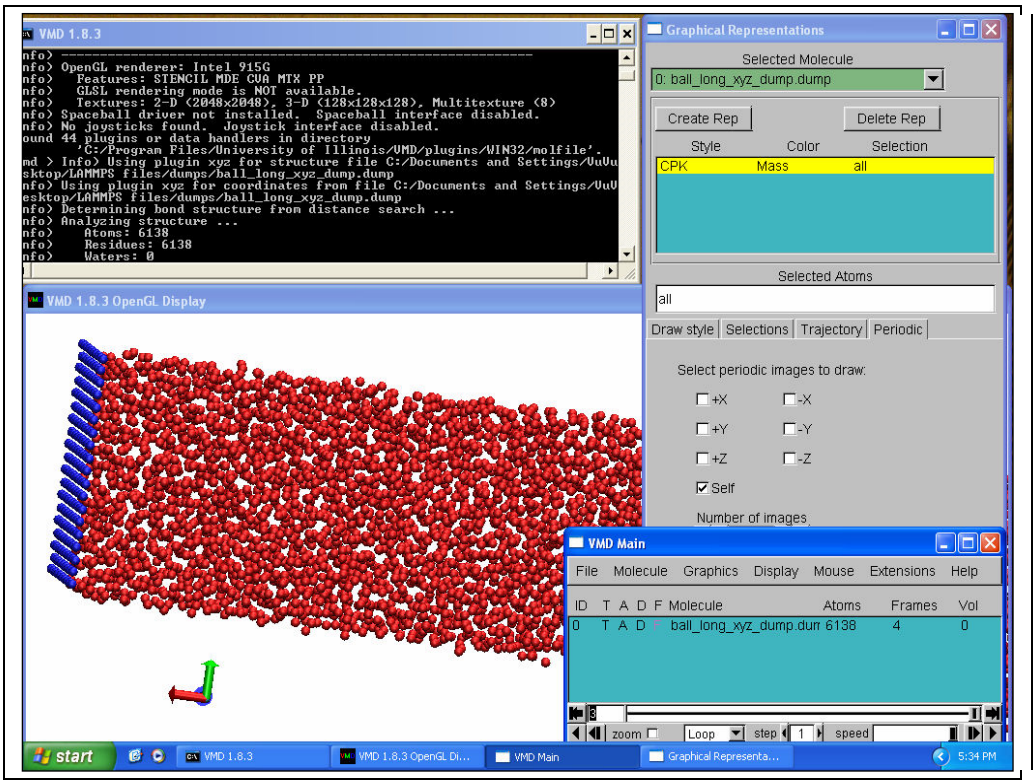

Figure 3.1. VMD interface. ***Illustrated under "Fair Use" copyright guidelines.***

Chapter 4: Development of Biosensor Inspired Problems

As discussed briefly in Chapter 1, drag on a nano-size sphere near a wall has interesting applications in biosensor design. In the future, BARC and FDB type biosensors could use nano-size beads to "label" the detection of a specific biological molecule in the same way that micron-size beads do today.

In the case of the BARC biosensor, a fluid containing single strand DNA is pumped through channels which are lined with complementary DNA strands. If a targeted biological agent is present, hybridized DNA pairs result. Beads are then pumped through the channel and bond to the hybridized pairs. The FDB operates similarly, except that sample single-strand DNA is attached directly to the bead rather than being pumped through the channel in a preliminary step. Any beads which are not bound are removed with magnetic (BARC) or fluidic (FDB) forces. The intensity of the remaining bonded beads label the presence of a targeted biological agent [Gijs, 2004].

A known limitation to any "bead labeling" approach is the background noise created from uncaptured beads, i.e., those unbound beads which remain in the biosensor while the bound beads are being counted. These unbound beads will be more numerous if the force required for removing the beads is not well understood, thus leading to the problems investigated in this thesis. A biosensor can be physically smaller if nano-size rather than micro-size beads are used as labels; however, the force needed to remove an unbound 'nanobead' is not well understood. This thesis takes a first step toward enabling the eventual use of nanobeads by investigating the drag forces which act on both a nanobead and a planar surface.

Insight into the magnetic or fluidic forces needed to remove unbounded beads can be gained by finding the drag on a single nanobead at different positions within the biodetector and at different Reynolds numbers. MEMS and NEMS devices have a large

surface to volume ratio, making the near-wall behavior of the bead and the skin friction on the inside surface of the biosensor important. In particular, knowledge of the following quantities is useful:

Problem 1: Drag acting on an isolated sphere. The drag coefficients of a nanosphere in an infinite fluid are found as a function of nanosphere velocity. A range of Reynolds numbers between 1.98 and 8.0 are considered.

Problem 2: Drag acting along a wall. The skin friction coefficients of a wall are determined for a variable wall density at a fixed velocity of $2.0\sigma/\tau$.

Problem 3: Drag acting on a sphere near a wall. The drag coefficients of a nanosphere near a wall are determined at a fixed velocity of $2.0\sigma/\tau$. Seven separate distances are considered.

Setting up, solving, and critically examining the results of these three basic problems is the goal of this thesis. The problems are divided into three sets of simulations, which will be termed "research runs". Before any research runs are carried out, LAMMPS will be applied to a validation problem of which the setup and simulation is the topic of Chapter 5.

Chapter 5: Validation of the LAMMPS Code

5.1 The Need for a Validation Problem

The validation case here was based on the work of Koplik et al. [1996] and described in Section 2.3. They used MD simulation to determine the drag on a nanosphere in an infinite fluid and compared these results with Stokes law. In this chapter, one of these drag calculations is repeated and compared with the results of Koplik et al. The details of the setup and simulation of this problem are described below.

5.2 Modeling Considerations

Koplik et al. [1996] describe a solid sphere, constructed from individual atoms, moving through an atomic liquid. Moving an object through a stationary fluid is unusual when compared to the "wind tunnel" approach typically used in experimental and computational aerodynamics in which fluid flows over an object. The field of MD developed independently of aerodynamics in the 1960s as a study of stationary fluids and gradually acquired a culture of fluid-centric rather than body-centric simulation. The two methods are equivalent; however, the traditional reference frame of a stationary fluid is used in this work[II].

Many of the parameters of Koplik et al. [1996] are duplicated in this thesis, with the notable exception of the simulation box dimensions and the need for a permeable vertical wall (both described later). As in the work of Koplik et al., nondimensional LJ units are used throughout the simulation. Length, temperature and mass are nondimensionalized with $\sigma = 3.4\text{Å}$, $\varepsilon/k_b = 120\text{K}$, and $m = 40$ amu, respectively. The natural time unit is then $\tau = \sigma\cdot\sqrt{(m/\varepsilon)} = 2.16\cdot10^{-12}$ sec.

[II] The simulation of Section 5.5 was modeled using both a stationary fluid and a moving fluid propelled by a piston. The two approaches yielded a drag result within 3% of one another.

The fluid of the problem is created first. Roughly 25,000 fluid atoms are assigned at points on an FCC lattice that completely fills the simulation box. Each fluid atom has a mass of 1m and all atoms interact via the LJ 12-6 potential function. The nondimensional density of $0.8m/\sigma^3$ and FCC structure of the fluid are identical to Koplik et al. [1996]. A void for placement of the sphere is created by deleting fluid atoms inside of a radius 2.1σ centered at X = 6, Y = 15, Z = 6 in the simulation box. See Figure 5.1 for coordinate system.

The sphere is duplicated from Koplik et al. [1996] by forming a separate FCC lattice with a density of $1.8\ m/\sigma^3$ and extracting the atoms inside a radius of 2σ. These 56 atoms are then centered in the void described above. Atoms in the sphere are not allowed to interact with each other but do interact with the fluid atoms with a LJ 12-6 potential. Interactions among the sphere atoms can cause a slow increase in radius which may influence the drag force. These atoms are given a very high mass of $1.8 \cdot 10^6 m$ for reasons explained in Section 5.4.

The two principal stages of the simulation will now be carried out. During the first stage, a crystalline solid will be melted to form a fluid. In MD literature, this process is known as "equilibration". Once the solid is completely melted, the sphere will travel through the fluid in a NEMD simulation.

5.3 Equilibration of the System

Atoms are initially melted from an FCC lattice by imposing a temperature on the solid that is above its melting point. A temperature of $1.2\varepsilon/k_B$ (144K) is applied in this case, giving atoms a sufficient kinetic energy to break the attractive bonds of the LJ potential and move around the simulation box.

After some time, all traces of the well ordered solid shown in Figure 5.1 are lost and replaced with random thermal motion – this occurs when the system has concluded

the equilibration process and reached a stable equilibrium state. The transformation to a liquid must be complete, thus requiring that the final temperature and density of the fluid lie within the liquid region of the phase diagram.

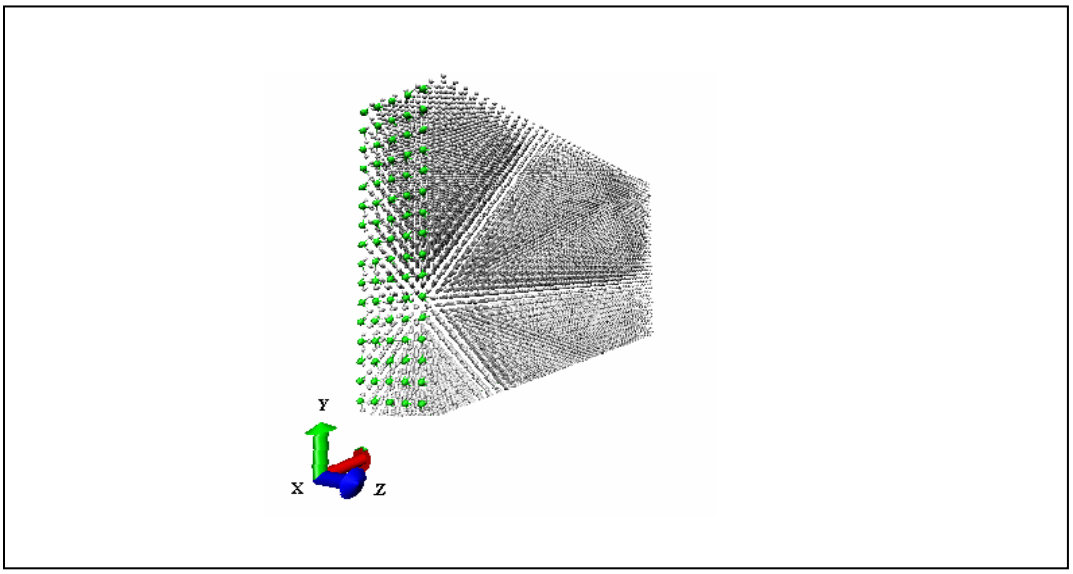

Figure 5.1. The fluidic system as a solid. Atoms are shown as enlarged points to illustrate the FCC lattice structure of the fluid. Stripes in the fluid are a result of the FCC lattice structure and do not indicate any nonuniformity in the atomic spacing.

Figure 5.1 shows the actual fluid system before the equilibration process was started. The need for the permeable wall shown on the left face of the simulation box is discussed in Section 5.4.

The achievement of an equilibrium state can be recognized by several markers. From a macroscopic (thermodynamic) point of view, the system's entropy must be a maximum. Unfortunately, entropy is not a physical quantity that lends itself to measurement and its direct calculation from the microcanonical ensemble is limited to trivial systems. However, it is possible to detect the attainment of an equilibrium state, with a reasonable degree of certainty, by the observation of other parameters [Haile, 1997].

One such observation is the fluctuation of instantaneous thermodynamic properties about a running average that is independent of the simulation time. Another requirement is that the time average of each atom's Cartesian component of velocity follow a Maxwell velocity distribution [Haile, 1997]. The Maxwell velocity distribution is a Gaussian distribution with standard deviation $s = (kT/m)^{1/2}$ and mean velocity $\langle v \rangle = 0$. It is defined as

$$\sqrt{\frac{m}{2\pi kT}}\, e^{\frac{mv^2}{2kT}} \tag{5.1}$$

where T is temperature of the fluid. One component of the velocity distribution of fluid atoms taken at the end of an equilibrium simulation is illustrated in Figure 5.2 below.

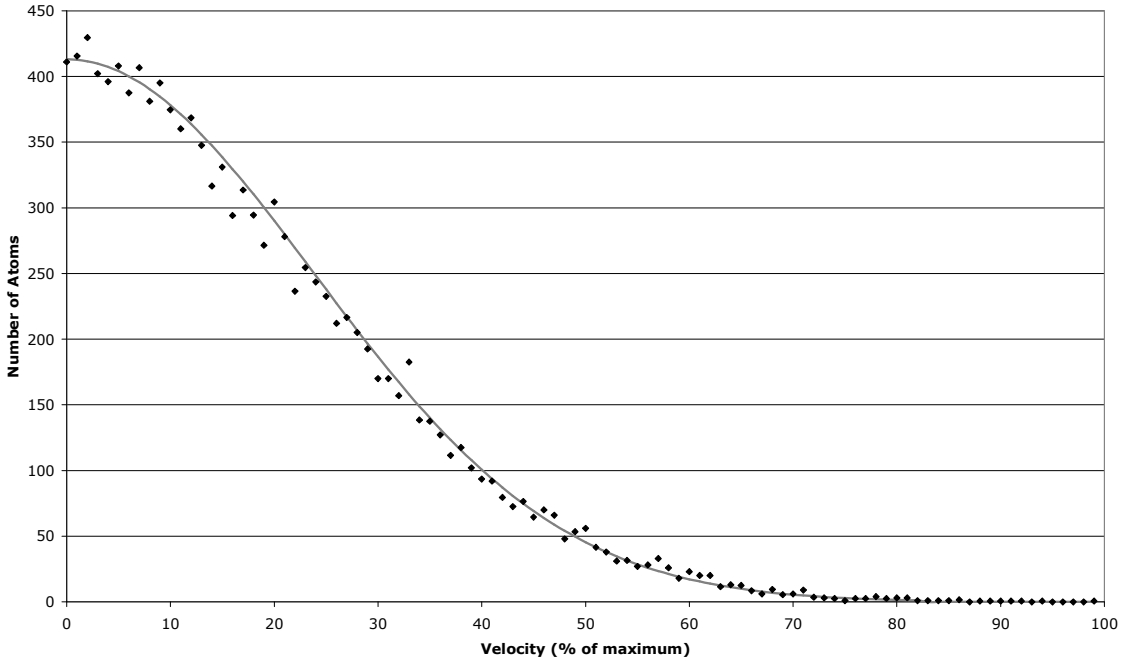

Figure 5.2. Velocity distribution of fluid atoms at 50τ (shown for one degree of freedom). The speeds predicted by the Maxwell distribution are shown with a solid line.

The Maxwell velocity distribution is shown only for positive velocities acting in the *X* direction. Negative velocities and velocities acting in other Cartesian directions have an identical Maxwell distribution.

The distribution shown in Figure 5.2 occurs after a time of 50τ. At this point, the temperature and pressure of the system were observed to show fluctuations with a magnitude less than 1% of the average. From combined inspection of thermodynamic properties and the velocity distribution, it was concluded that the system was equilibrated.

Comment: The interpretation of the sphere's radius must now be adjusted since the radius inaccessible to fluid is different than the radius created in Section 5.2. As discussed in Chapter 1, atoms behaving according to the LJ potential experience a rapidly increasing repulsive force when moving within roughly 1σ of another atom. Atoms on the surface of the sphere apply this repulsive force to nearby fluid atoms and therefore cause the sphere to behave as if the radius has been increased by 1σ. Figure 5.3 below illustrates how the "nominal" radius of the sphere is measured.

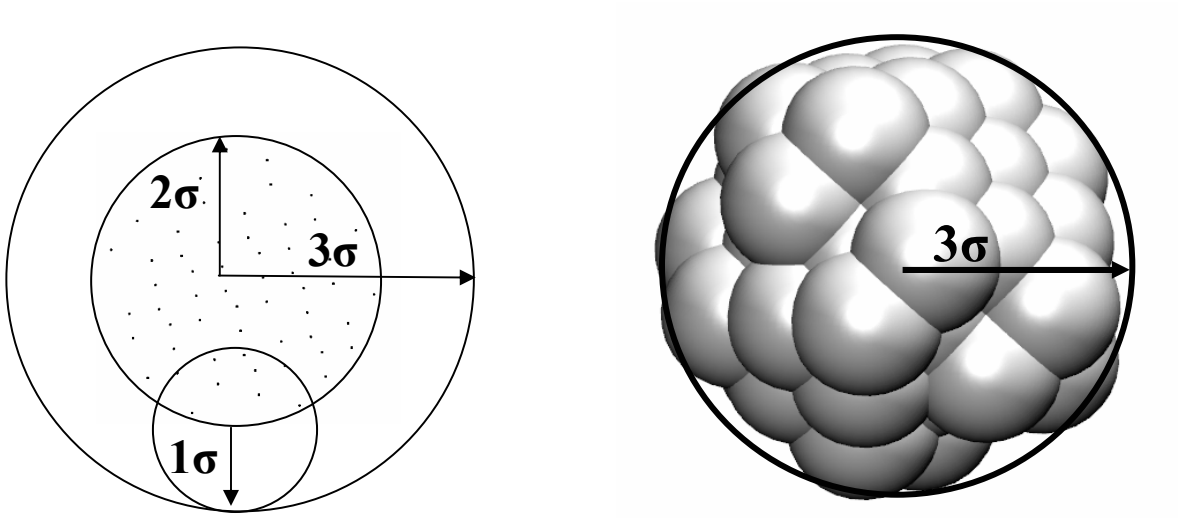

Figure 5.3. The coordinates of the atoms (A) and their repulsive force fields (B). Small spheres represent volumes inside the LJ repulsive core that are not accessible to the fluid.

5.4 NEMD Simulation

The sphere is given an initial velocity of $2.0\sigma/\tau$ and allowed to move across the simulation box for a time of 35τ. This is the same speed used by Koplik et al. [1996] and corresponds to a Reynolds number of Re = 4.95 based on sphere diameter. Because of the sphere's large mass, the velocity (and momentum) of the sphere is nearly constant throughout the simulation despite the drag force acting against its motion. Nonetheless, some momentum is still deposited into the fluid by the sphere. A velocity rescaling type thermostat adjusts the kinetic energy of the fluid so that a constant temperature is maintained. Section 1.8 provides a description of this thermostat.

In an MD simulation, finding the instantaneous drag on an object is straightforward since the forces on each atom are known at every timestep. In this case, the component of force parallel to the sphere's movement is summed for each atom of the sphere to yield the net instantaneous drag force.

Using completely periodic boundaries on the simulation box caused the sphere to experience a drag force with a magnitude that was too small. The momentum in the direction of the sphere's movement exited the simulation box in front of the sphere and reentered behind it. This circulation of fluid caused the magnitude of the drag force to continuously decrease as the sphere moved further along the simulation box. Placing a solid wall at the end of simulation box could have completely prevented the momentum transfer; however, the simulation results of this author found that the drag force's magnitude increased with the presence of a solid wall. Analytical results [Brenner, 1961] also show that a sphere moving perpendicular to a solid wall will experience an increased drag as it approaches the wall. For this reason, a hybrid method was used to allow some, but not all, of the fluid momentum to move through the wall.

A permeable vertical wall filled this role by acting as a screen that reduces the flow rate around the simulation box. The permeable wall was constructed from a single layer of atoms in a BCC lattice having with a density of 0.8 m/σ^3. Atoms of the wall are not allowed to interact among themselves and were given a large mass of $1.8 \cdot 10^6 m$ so that they do not move throughout the simulation. Interactions between the fluid and permeable wall are governed by the same LJ potential as the fluid-fluid interactions. The complete system is shown in Figure 5.4 below.

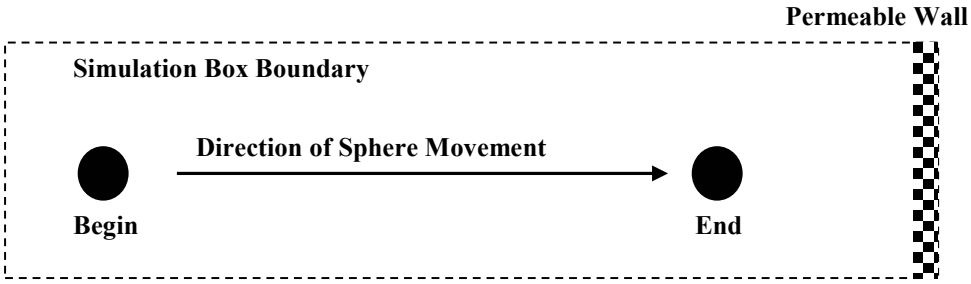

Figure 5.4. Geometry of the simulation after the addition of a permeable wall at the end of the simulation box.

While using the setup shown in Figure 5.4, it was observed that the drag force on the sphere remained at a time invariant (steady-state) value when the sphere was near the center of the simulation box.

5.5 Validation Results

Although the sphere is moved through the fluid for a total time of 35τ, the first 15τ (a distance of 30σ) is needed to yield a steady-state drag value. Drag data is considered only after the initial transient period has passed and before the sphere approaches the permeable wall. As in Koplik et al. [1996], the drag force is sampled every 0.25τ and the mean drag force is calculated over 12.5τ. The mean drag as a function of time is shown in Figure 5.5 (solid line).

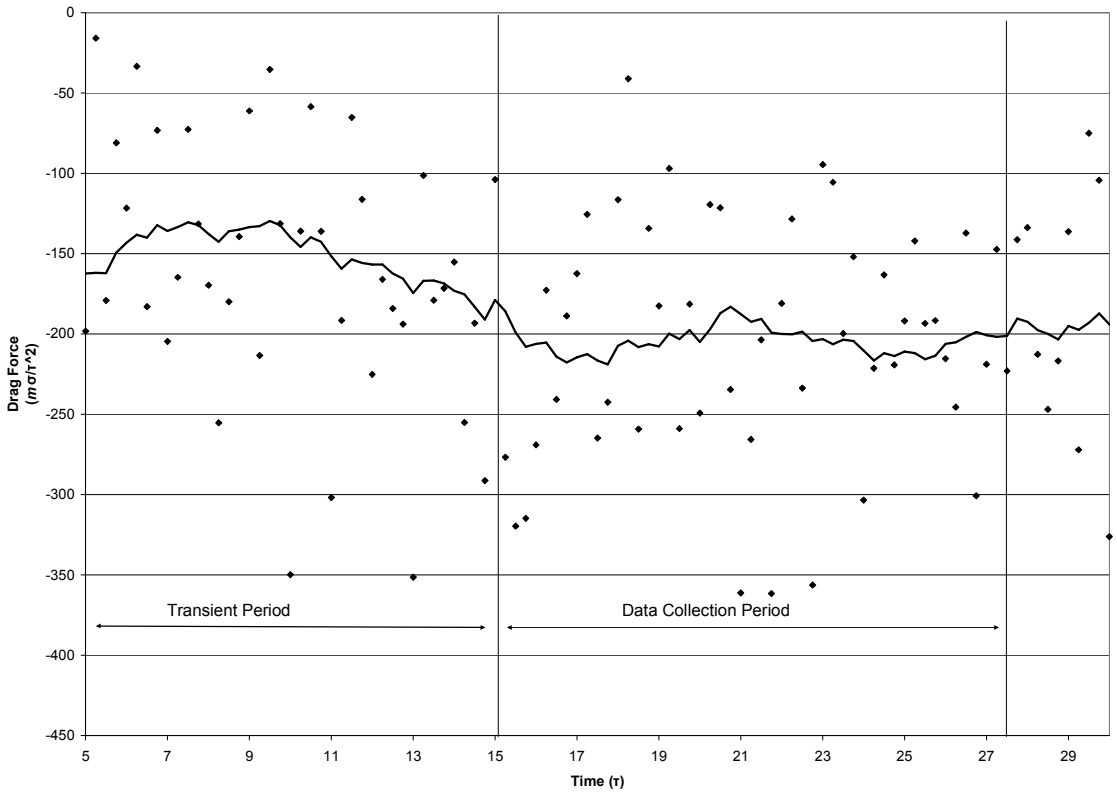

Figure 5.5. Transition to Steady-State Drag at Re = 4.95. Instantaneous drag measurements are shown as diamonds.

The variation of the instantaneous drag force is not intuitive. Despite the sphere's composition of 56 individual atoms, with many of those being exposed to the fluid, the drag force in Figure 5.5 (shown as diamonds) rarely resembles the running average of the drag force (solid line). Our confidence can be improved by putting these results in a statistical context. An analysis (not shown) of the "Data Collection Period" in Figure 5.5 reveals that the drag data follows a roughly Gaussian distribution which has a mean equal to the running average. A uniform distribution would be expected if the drag data occurred randomly.

To form a comparison with Koplik et al. [1996], the mean drag will be expressed as a computed radius obtained with Stokes law. The drag acting on the sphere in the steady-state condition leads to a computed radius of 2.816σ. This is 7% less than the nominal radius of 3σ and 10% less than the computed radius of $3.1\pm0.3\sigma$ reported by Koplik et al.

The computed radius found by Koplik et al. has an uncertainty large enough to include the computed radius of this validation problem. It is therefore concluded that the drag results calculated here are reasonable and that the problem-solving approach taken in this chapter will yield valid drag results for the problems discussed in Chapter 4.

Comment: Although the results of this thesis and Koplik et al. are within the limits of uncertainty, a possible explanation for the larger radius of Koplik et al. comes from the setup of the problem. Rather than terminating the simulation box with a permeable wall, a solid wall was used. Koplik et al. state that the simulation box is long enough to ignore boundary effects. The simulations of this research did not lead to the same conclusion – a solid wall was seen to increase the drag force significantly during the final 30% of the simulation.

Chapter 6: Setup of the Research Runs

Before presenting the results of the research runs, it will be helpful to discuss a few aspects of the modeling that will be needed to carry out these calculations. First, those elements of the research runs which are in common with the validation case discussed in the previous chapter are described. Then, since Problems 2 and 3 require the addition of a wall to the simulation, how this is done will be described. Following this, the sizing of the computational region will be described. Finally, because each research run will later be compared with results of a Navier-Stokes solution, the chapter concludes with a consideration of various issues which are related to the validity of that comparison.

6.1 Similarities with the Validation Case

The production runs and the validation case have much in common. In particular, the design and placement of the sphere and permeable wall are taken directly from the validation case. In addition, the fluid properties, the fluid equilibration process, and the fluid thermostat are also identical to those used in Chapter 5.

As in Chapter 5, the collection of drag data begins with sphere's center at a distance of 6σ from the front edge of the simulation box and a constant drag value is observed after a distance of 30σ has been traveled. The drag force in each research run is then sampled every 0.25τ over 12.5τ[III] and averaged to produce a mean drag force.

6.2 The Modeling of the Wall

The wall was modeled by a collection of roughly 2000 atoms that interact with the fluid using the 12-6 LJ potential but do not interact with each other. The wall was built with an FCC lattice structure that has a different density in each of the five simulations of

[III] At Re = 8.0, the distance needed to reach a steady-state drag force is less than 30σ. The shorter approach to steady state allows an additional length of simulation box to be used for measuring the steady-state drag. By traveling this additional length, the sphere is able to meet the time requirement of 12.5τ in a steady state condition.

Problem 2 and a fixed density in Problem 3. No roughness beyond the discreteness of the atoms is introduced and, like the atoms in the sphere, the wall atoms were given large, non-physical masses of $1.8 \cdot 10^6 m$.

The wall is located at the bottom of the simulation box and has a thickness of two atomic layers to prevent the fluid near the upper boundary of the simulation box from influencing fluid near the lower boundary via periodic boundary conditions. Using a double-layer wall provides more fluid separation than the LJ potential cutoff of 2.5σ, meaning that fluid atoms cannot interact with other fluid atoms through the wall. The position of the wall is shown below without fluid present (A) and in a diagram of the simulation box (B).

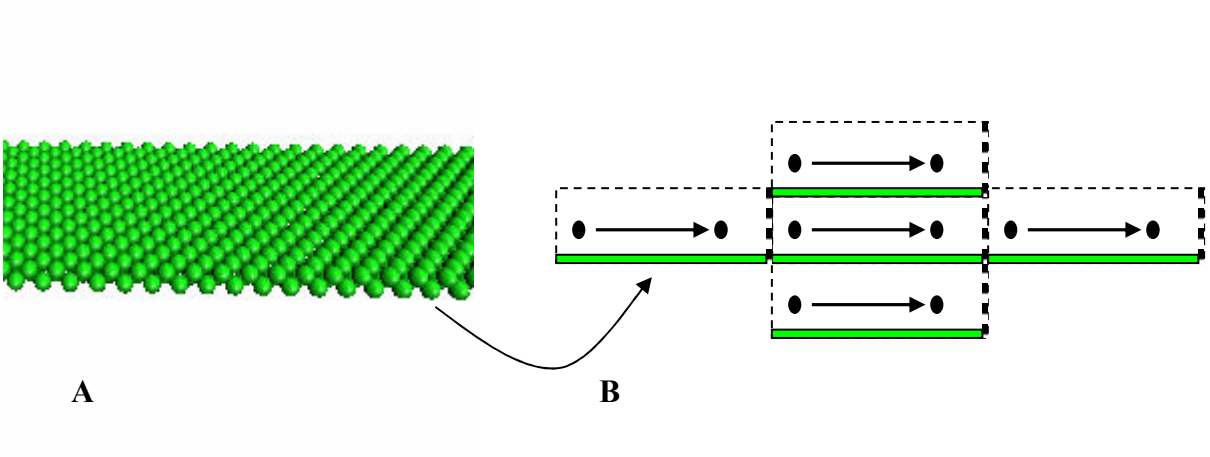

Figure 6.1. The atomic wall of density 1.8 N/σ^3 with FCC packing structure (A) is located at the bottom of the simulation box and duplicated by periodic boundary conditions (B).

It must be noted that the wall and sphere used in the research runs are not intended to represent specific materials. At the temperature and pressure of the simulation, a more complex potential function or quantum mechanical approach is needed to form a real solid and atomic separations are, in turn, governed by such considerations. Solids using these complex potentials are computationally more

expensive than the LJ solids used in these simulations. Accuracy then has been traded for simplicity.

In this connection, it is important to realize that the sphere used here (and the wall as well) could not remain intact if the atoms were assigned a smaller, more physical mass and allowed to interact with one another. The atomic spacing is smaller than preferred by the LJ potential, and if left unchecked would cause the sphere to expand into the fluid. As described in Chapter 5, the expansion of the sphere is easily prevented by turning off the interactions among the sphere atoms, and this procedure is again used here.

Since the wall (and the sphere) are not actual materials, this introduces the atomic density of the wall as another variable. Thus in the description of the results of Problem 2 in Chapter 7, the density of the wall will be treated as a variable.

Varying the density of the wall has consequences. The drag force on a body whose atoms behave according to a two-body potential will depend heavily on the number density used. Each fluid atom near the surface must interact with all the surface atoms within its cutoff radius, thus resulting in a stronger fluid-surface interaction as number density increases.

6.3 Sizing the Simulation Box

For the sake of consistency, it was decided to use the same size simulation box for all of the three problems. The size of the simulation box must therefore meet the needs of all problems. The considerations which resulted in the simulation box having dimensions of $70\sigma x40\sigma x12\sigma$ will be described in the following paragraphs.

The length of the simulation box is the dimension parallel to movement of the sphere. It is sized by considering the distance required by the sphere to reach and maintain a steady-state drag force. The validation problem of Chapter 5 requires steady-state drag to be maintained for 12.5τ; the same standard is applied here. As described in

Section 5.5, the sphere is observed to develop a steady-state drag after a distance of 30σ (15τ), meaning that a total runtime of 27.5τ and a total length of 55σ is required. A length of 6σ is added to this minimum requirement since the sphere does not start at the beginning of the simulation box and an additional 9σ is added so that larger Reynolds numbers can be accommodated. The total length of 70σ was found to be large enough to allow a reliable measurement of drag force in the above sense for all three cases.

The height of simulation box is the dimension perpendicular to plane of the bottom wall. A simulation box with a height greater than that used in the work of Koplik et al. [1996] was needed to negate the effect of the wall's replica appearing *above* the simulation box as shown in Figure 6.1B above. The combination of the two walls results in what is effectively Poiseuille flow with a slip condition at the walls. The "upper" wall, a product of the periodic boundary conditions, must have a large enough separation from the lower wall so as not to significantly affect flow patterns in the bottom half of the simulation box. The required height is found by increasing the displacement of the two walls until the drag on a sphere at the center of the simulation box matches the results obtained in Chapter 5, which correspond to an infinite wall separation. A total required height of 30σ was found to be necessary to assure this and an extra 10σ was added as a safety factor.

The width of the simulation box (12σ) was small in comparison with its length and width. It needs only to be wide enough so that the effect of the periodic boundary conditions does not substantially interfere with the drag force. It was assumed that the 12σ width used by Koplik [1996] was sufficient for this purpose.

6.4 Comparing with Continuum Results

The author is not aware of any MD simulations with which Problems 2 and 3 can be compared. In their absence, one alternative is to compare with Navier-Stokes solutions of similar problems. This comparison needs to be viewed with care.

One issue is the adequacy of a continuum solution for these problems. Fortunately, the Knudsen number (the ratio of the mean free path to the characteristic dimension of the problem) is high enough (0.01 to 0.1) so that this is not a concern. In this Knudsen number range, both the Navier Stokes (continuum) solutions and the MD (particulate) solutions to these problems are valid.

The issue of the proper choice of boundary conditions to be employed in the Navier Stokes calculations is more problematic. This is because in this range of Knudsen number neither no-slip or pure slip boundary conditions are appropriate [Panton, 2005], but rather something in-between, and the author is unaware of any rigorous way of determining just what the appropriate boundary condition would be[IV]. In the following chapter, comparison with Navier Stokes solutions employing both no-slip and pure slip boundary conditions are made with the intent of providing reasonable limits with which the MD simulations can be compared.

[IV] Using MD simulation does not resolve this problem, unless a potential which represents the actual solid-fluid interaction is used. In this work the same potential was used for the solid-fluid interaction as for the fluid-fluid interaction.

Chapter 7: Results of the Research Runs

Information concerning the results for each of the three Research Runs can be found in this chapter. To build confidence in the results, they are compared with the MD solutions of similar problems where possible and with Navier Stokes solutions in the cases where an MD solution is not available.

7.1 Problem 1: Drag on an Isolated Sphere

This section describes the problem of calculating drag on a nanosphere in an infinite fluid. This problem is identical to validation problem of Chapter 5, the only difference being that the simulation has been carried out for six Reynolds numbers between 1.98 and 8.0, rather than a single Reynolds number of 4.95. The results are shown in Figure 7.1.

Good agreement with the results of Koplik et al. is seen at both of the Reynolds numbers used in their calculations (1.98 and 4.95). Data at Reynolds numbers less than Re = 1.98 could not be collected due to a large uncertainty in the mean drag force. This is because at a low velocity, the magnitude of the drag force on the sphere is comparable with thermal noise caused by interactions with fluid atoms. Extracting useful data becomes impossible in this condition.

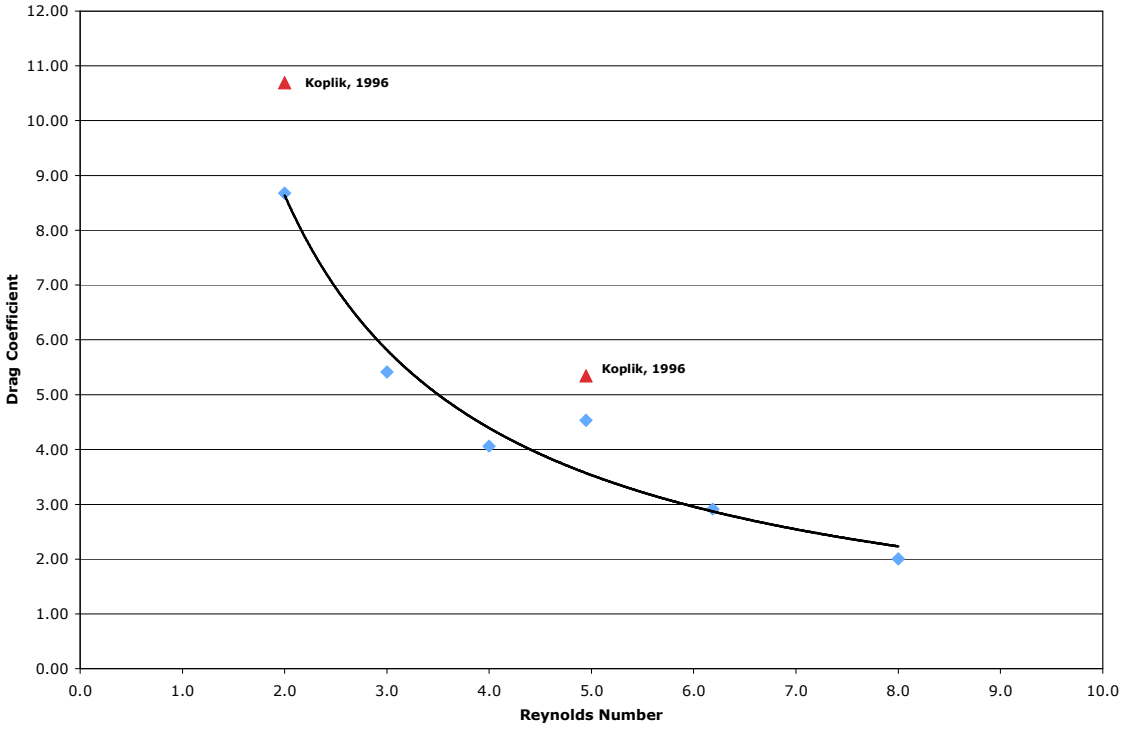

Figure 7.1. Drag coefficient of a nanosphere at several Reynolds numbers.

To better understand the nature of the boundary conditions, it is useful to compare these results with two Navier Stokes solutions; one employing no-slip and the other a variable slip boundary condition. The no-slip result is given by the well-known Stokes solution while the variable (between pure slip and no-slip) result is given by the work of Happel et al [1967]. Both the Stokes and the Happel et al. results can be considered (for their particular boundary conditions) *minimum* drag results since they correspond to conditions of very low Reynolds numbers. Figure 7.2 illustrates Stokes law, the Happel et al. results for a *pure* slip condition and the MD results.

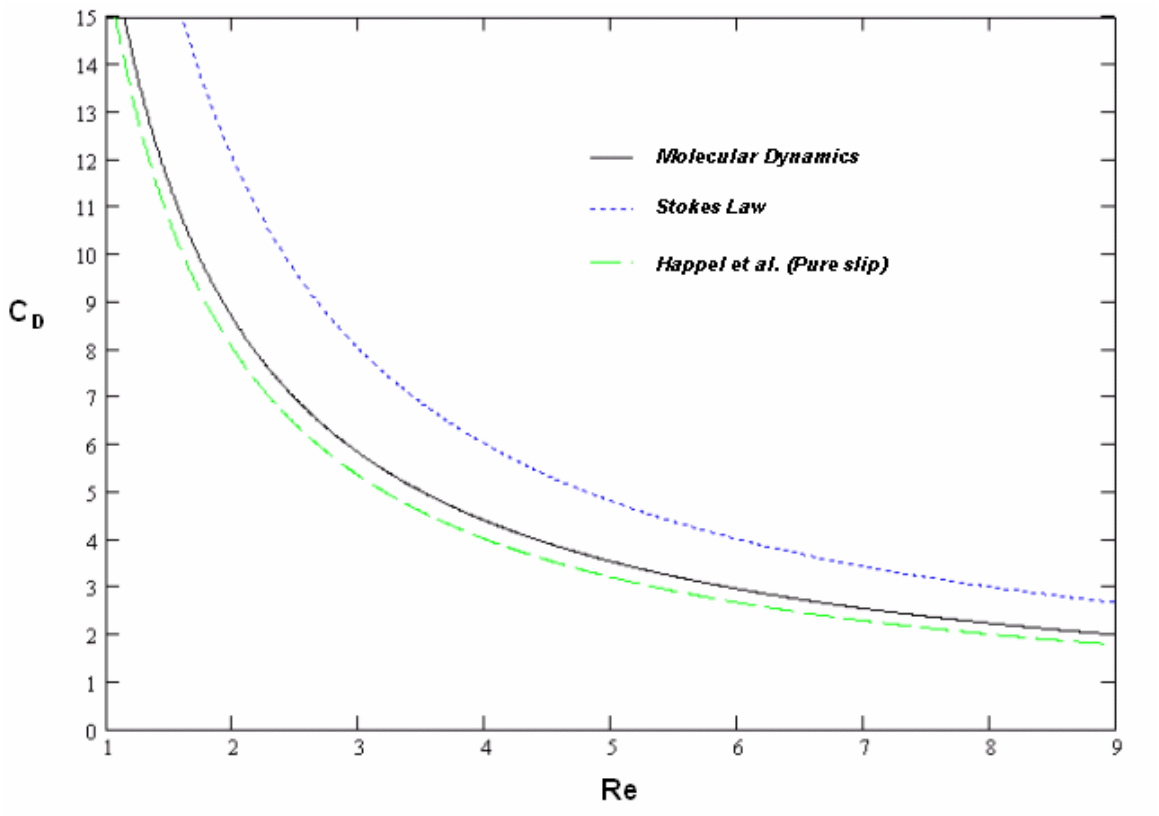

Figure 7.2. Drag force as a function of Re from MD and Navier-Stokes equations.

As discussed in Section 6.5, the Knudsen number of this simulation indicates that some slip is present, thus suggesting a lower drag value than that given by Stokes law. This is in fact observed in Figure 7.2. Further, Figure 7.2 indicates that the values of drag obtained in this problem are greater than the pure slip results, as they must be. Clearly this supports the Knudsen-number-based argument of Chapter 6 in which a boundary condition between that of pure slip and no-slip should be expected. Further supporting this argument is the fact that a visualization of the sphere using the VMD tool described in Chapter 3 shows that the fluid atoms slip along the sphere's surface. The fluid behavior appears as a continuous slip – not the stick/slip mechanism sometimes observed experimentally in microfluidics.

The drag coefficients from MD simulation are very close to the pure slip condition (bottom curve) in Figure 7.2. This is interesting since the Knudsen number of the flow suggests a boundary condition more near to a no-slip condition than a pure slip condition. The qualitative nature of the Knudsen number argument may contribute to this difference as well as need for an improved fluid-solid interaction in the MD simulation.

7.2 Problem 2: Friction on a Wall

This section describes the problem of calculating the friction along a wall as a function of the wall's number density.

Friction is evaluated along the length of the simulation box by moving the entire wall through the fluid at a velocity of $2.0\sigma/\tau$ but only observing forces on the atoms within a 6σ x 6σ sample area. The instantaneous friction is found by summing the horizontal force on each atom in the sample area, which is similar to the drag calculations in Chapter 5 except that the friction is evaluated on only a portion of the wall. Only half of the friction is used to calculate a skin friction coefficient since periodic boundary conditions cause the fluid to exert force on both sides of the wall.

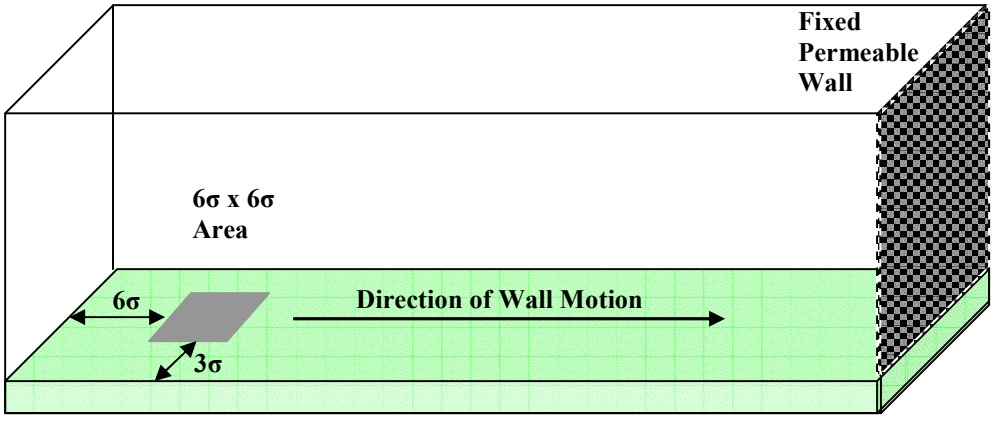

Figure 7.3. Position and motion of the wall.

When the wall (initially at rest) is given a fixed velocity, the friction displays a transient behavior similar to the sphere of validation problem and then settles into a steady-state behavior which is independent of the computational time. Figure 7.4 illustrates the steady-state skin friction coefficient as the density of the wall is varied from 1.0 to 5.0 N/σ^3 in intervals of 1.0 N/σ^3. Drag is expressed as the skin friction coefficient, defined as

$$C_f = \frac{F}{\frac{1}{2}\rho A U^2} \tag{7.1}$$

where ρ is the density, U is the fluid speed, A is the sample area and F is the friction acting on the sample area.

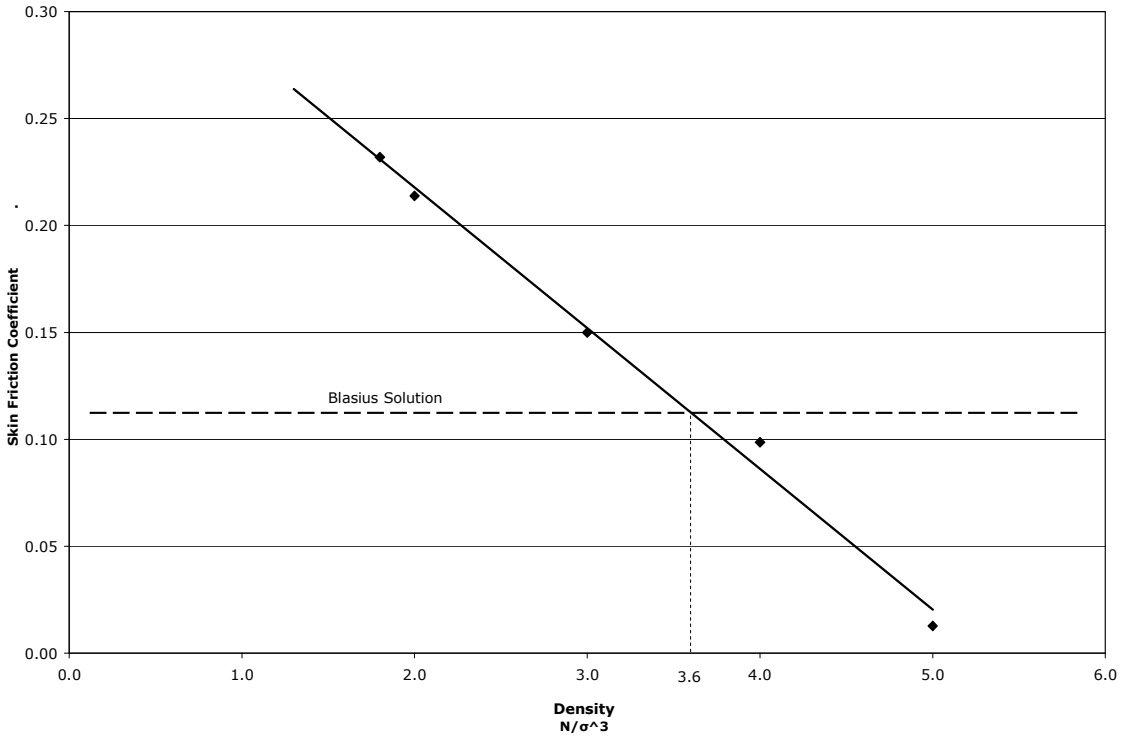

Figure 7.4. Relationship of drag coefficient and number density for a Lennard-Jones wall.

The linear dependence of the skin friction on density was expected since the number density of the solid is directly proportional to the number of wall-fluid interactions (forces) at the solid's surface.

Although the Knudsen number of this problem indicates that a slip condition is more appropriate, a comparison with a known analytical solution can give perspective to the skin friction coefficients found here. The Blasius solution, which describes the behavior that would be expected in a similar continuum problem if the no-slip condition were applicable, can predict the drag coefficient as a function of the sample area's displacement from the front edge or "leading edge" of the simulation box. The skin friction coefficient as determined from the Blasius solution is given by the following relationship:

$$C_f(x) = \frac{0.664}{\sqrt{Re(x)}} \tag{7.2}$$

This expression is valid for laminar flows only [Panton, 2005]. A maximum Reynolds number of Re = 44.5 is calculated for the flow in this problem – well within the limits of laminar flow.

The characteristic length applicable to the Reynolds number in the Blasius solution is the distance from the leading edge of the plate, thus a mean skin friction coefficient can be obtained by evaluating the integral average of Equation 7.2 between 30σ and 54σ. The mean skin friction coefficient of the Blasius solution was found to be $C_f = 0.114$.

It is interesting that the Blasius result may be matched to an effective wall density as shown in Figure 7.4. Although a wall of this number density will produce the same mean drag coefficient as predicted by the Blasius solution, it does not produce the position dependent boundary layer also predicted by the Blasius solution. All of the skin friction coefficients determined here were seen to be independent of position.

Comment: During equilibration, a VMD visualization showed fluid atoms forming loosely ordered layers near the surface of the wall. Voids between these layers were especially obvious surrounding the 1st and 2nd layer of fluid. It is likely that that a similar phenomenon exists around the sphere of Section 7.1, however, a visualization of the solid-liquid interaction is more difficult since the fluid completely surrounds the sphere.

7.3 Problem 3: Drag on a Sphere near a Wall

This section describes the problem of calculating the drag on a sphere near a wall as a function of the sphere-wall separation. The geometry is a combination of Problem 1 and Problem 2; however, the wall is now created with a constant density which is equal to that of the sphere of Problem 1. There is no relative motion between the sphere and the wall – both move simultaneously through the fluid at a speed of $2.0\sigma/\tau$ (Re_{sphere} = 4.95).

Drag on the sphere is measured at seven sphere-wall separations which ranged from 26σ to zero. At a separation of zero, the lowest atom of the sphere is allowed to contact an upper atom of the wall. Figure 7.5 shows the resulting drag coefficients and their corresponding sphere-wall separation.

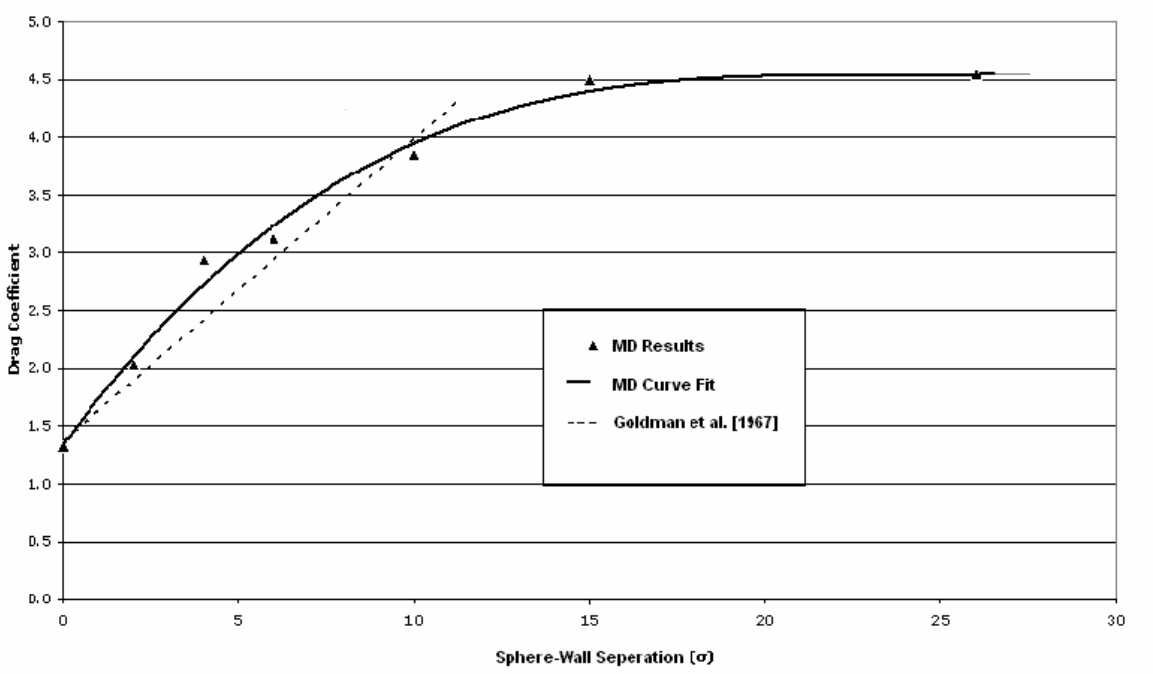

Figure 7.5. Drag coefficient of a sphere as a function of separation from a wall. Analytical results are from Goldman [1967].

The drag at a sphere-wall separation of 15σ and greater is essentially the drag of a sphere in an infinite fluid and corresponds to the results of Section 7.1 (at Re = 4.95). As seen in Figure 7.5 above, the drag of the sphere decreases as it approaches the wall until reaching a minimum when in contact with the wall. Numerical results in the continuum regime from Sandberg [2002] (not shown) also indicate that a sphere affixed to a wall experiences a significantly reduced drag force compared with the drag of a sphere in the freestream.

Goldman et al. [1967] found an analytical solution for the drag on a stationary sphere as a function of distance from a stationary wall. In Goldman's case the velocity profile is linear (uniform shear flow), which contrasts with the parabolic velocity profile of this problem[V]. In order to compare with Goldman et al., an equivalent linear velocity

[V] The parabolic profile is a result of periodic boundary conditions producing a second wall above the simulation box. These walls both drive the flow, thus creating a velocity profile similar to Poiseuille flow.

profile is needed. The equivalent linear shear in this problem will be taken as the average rate of change of velocity between the wall and the half-height of the simulation box[VI]. Using the equivalent linear profile in Goldman's solution produces the drag coefficients which are represented by the dashed line in Figure 7.5.

The results of Goldman et al. and MD are in surprisingly close agreement for small sphere-wall separations, especially when the sphere is in contact with the wall. This agreement is interesting since the fluid has a minimum Knudsen number which suggests the use of a slip condition rather than the no-slip condition used by Goldman. It is speculated that, in this problem, errors associated with forming an equivalent linear velocity profile cause the two results to agree more closely than would otherwise be expected. A more accurate comparison with results that employ a no-slip condition (such as a numerical solution of the Navier-Stokes equations), would likely yield drag coefficients that are greater than those of the MD solution.

Clearly, the Goldman results do not match well with the MD results as the sphere moves away from the wall and into the center of the channel; however, a close match of the two results cannot be expected since the linear and parabolic velocity profiles are much different in this region.

[VI] The no-slip condition is assumed at the wall.

Chapter 8: Suggestions for Future Work

This work considers a range of Reynolds numbers (1.98 to 8.0) guided by the work of Koplik et al. [1996]. In practice, the Reynolds number of flows on the micro- or nano- scale is usually much less than 1.0 and often less than 0.1. If we find the velocity from the median Reynolds number, we see that the sphere moves at a surprising 314 meters per second - obviously the Reynolds number of this flow would be much larger if not for the very small size of the sphere. A new set of simulations are needed to the determine drag coefficients of both an isolated nanobead and a nanobead near a wall at much lower velocities.

As discussed in Section 7.1, determining the drag force on a sphere in a low Reynolds number flow is difficult with the "translating sphere" approach taken by Koplik et al. [1996]. A new approach must be found so that physically useful (low Re) results can be produced. To avoid the problems of drag force measurement in low Reynolds number flows, it is desirable to eliminate as many variables as possible that influence the drag result, including the permeable wall and the limited running time of the simulation. Two alternatives exist that would meet these needs.

A NEMD simulation of a fluid moving around a stationary sphere would allow the instantaneous drag force to be monitored for any amount of time and would not require a permeable wall to be present. In this setup, fluid travels through the front of the simulation box, over the sphere, out the end of the simulation box and returns to the beginning via periodic boundary conditions. The fluid is reset to the freestream conditions before approaching the sphere. This simulation is the equivalent of the experimental device typically used in continuum regime fluid dynamics, i.e., the wind tunnel.

As a second approach, the Einstein-Stokes relation provides an opportunity to establish the drag force on a sphere with no bulk movement of the sphere or fluid and without a thermostat. This result, from Einstein's famous study of Brownian motion in 1905, relates the diffusion coefficient to the drag coefficient of an object in a low Reynolds number flow. A simulation using this approach has the great advantage that the diffusion coefficient may be measured in an equilibrium simulation. The system would be thermodynamically closed meaning that it conserves energy without a thermostat, thus simplifying the dynamics of the problem. The atoms of this system can also move forward in time indefinitely, therefore allowing temporal effects to be removed from the value of the diffusion coefficient.

Both of these alternative approaches rely on accurate potential models for the solid-fluid interactions. These potential functions are always estimates. Interactions on the atomic scale are fundamentally multi-body in nature rather than the often used assumption of a two-body interaction. The two-body assumption can produce good results under the right conditions and some potentials, such as the Embedded Atom Method (EAM) have had success combining two-body and multi-body interactions. Nonetheless, a potential that closely estimates the actual interaction of a solid and liquid is not available and requires further investigation.

Appendix

As noted in Chapter 1, molecular dynamics often uses time averages to measure thermodynamic properties in the microcanonical ensemble. A reasonable question arises: Why can these properties not be determined analytically from an ensemble average? After all, statistical mechanics provides a mathematical foundation for calculating macroscopic properties from microscopic states.

In some cases, macroscopic properties *can* be found analytically by working within an ensemble, i.e. an imaginary collection of systems all having the same macroscopic state. An example is the microcanonical ensemble discussed in Chapter 1.

A system of fluid contained in an insulated volume forms a good example of the microcanonical, or Number Volume Energy ensemble. The volume of fluid is fixed and has a constant number of atoms and a constant energy. This system's "configuration", i.e., the position and velocity of all its atoms, belongs to a large collection of other configurations which all have the same energy.

Derivation of classical thermodynamic properties from the microcanonical ensemble is straight forward in concept. Some form of counting allows the number of configurations with a given energy to be determined. The microcanonical partition function or multiplicity function, Ω(N,V,E), can be thought of as the number of configurations accessible to a given energy, with 1/Ω being the probability of observing a particular configuration. The microcanonical ensemble is related to classical thermodynamics using the *fundamental relation*,

$$S(N,V,E) = k_B \ln \Omega(N,V,E) \tag{A.1}$$

where S is the system's entropy. This is substituted into the classical thermodynamic relationships to yield thermodynamic properties:

$$\frac{1}{T} = k_B \left(\frac{\delta \ln \Omega}{\delta E} \right)_{N,V} \tag{A.2}$$

$$\frac{P}{T} = k_B \left(\frac{\delta \ln \Omega}{\delta V} \right)_{N,E} \tag{A.3}$$

A problem carrying out the above analysis arises when Ω is evaluated for a system of many particles. Since Ω represents the number of accessible states, it is an increasing nonlinear function of the system size that approaches infinity quickly. This classic problem limits the microcanonical ensemble's use in statistical physics and can be illustrated with a trivial example.

Consider a system of N particles that take on only two states: a ground state, s =0, and an excited state, s=1. To evaluate the multiplicity function, the number of states compatible with a system energy E must be found. The number of accessible states can be determined directly by counting how many ways that $m = E/N$ excited particles can be distributed in N total particles, or more simply a combination,

$$\Omega(E) = \binom{N}{m} = \frac{N!}{m!\,(N-m)!} \tag{A.4}$$

For simplicity assume half of the particles are in excited states, $E = ½\, N$. A plot of this function shows an exponential dependence of accessible microstates on the number of particles.

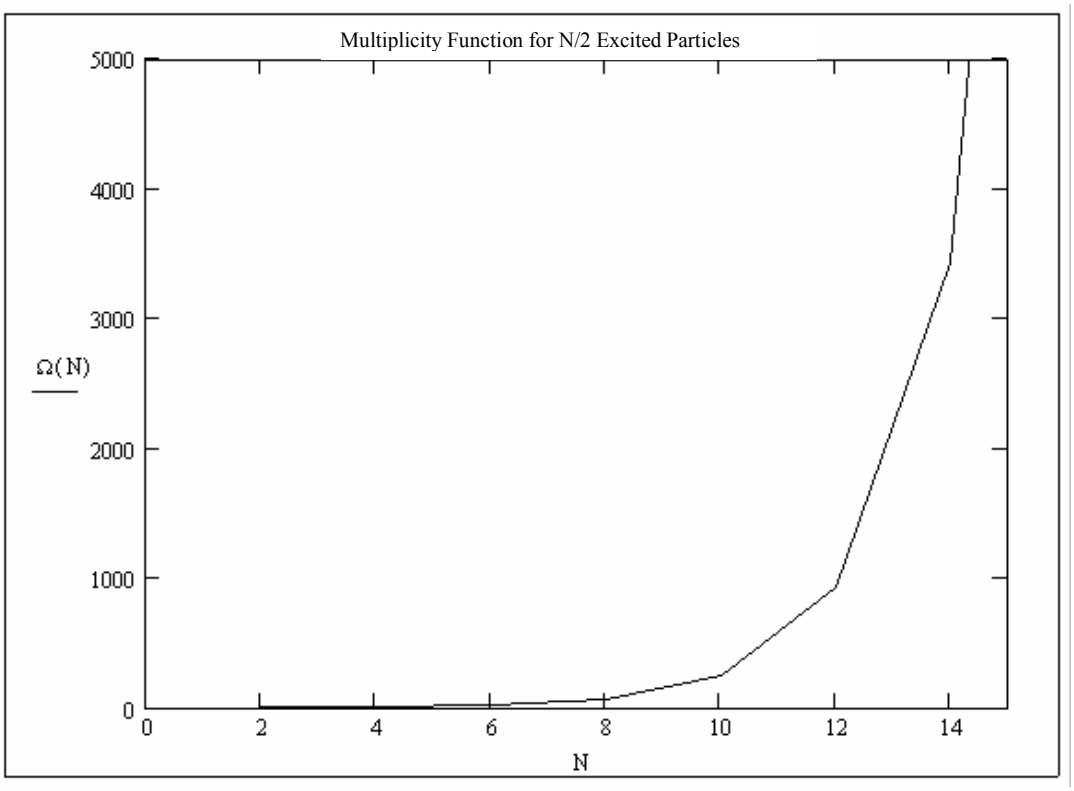

Figure A.1. The number of accessible states increases sharply with increasing particle number.

Notice that a small increase in the number of particles allows many more microstates (configurations) to become available. A realistic fluid simulation contains a minimum of several thousand particles, yielding a near infinite number of states. These large values make direct computation of thermodynamic properties impossible.

References

Abraham, F.1978. The interface density profile of Lennard-Jones fluid in contact with a Lennard-Jones wall and its relationship to idealized fluid/wall system: A Monte Carlo simulation. *Journal of Chemical Physics* 68:3713-3716.

Bocquet, Lyderic and J. Barrat. 1994. Hydrodynamic boundary conditions, correlation functions, and Kubo relations for confined fluids. *Physics Review* E 49:3079-3092.

Born, M., R. Oppenheimer. 1927. Ann Phys. 84:457-484.

Brenner, H. 1961. The slow motion of a sphere through a viscous fluid towards a plane surface. *Chemical Engineering Science* 16:242-261.

Cieplak, Marek, J. Koplik and J. Banavar. 2001. Boundary Conditions at a Fluid-Solid Interface. *Physical Review Letters* 86:803-806.

Gijs, M. 2004. Magnetic bead handling on-chip: new opportunities for analytical applications. *Microfluid Nanofluid* 1:22-40.

Goldman, A., R. Cox and H. Brenner. 1967. Slow viscous flow of a sphere parallel to a plane wall-II Couette flow. *Chemical Engineering Science* 22:653-660.

Guan, P., D. Mckenzie and B. Pailthorpe. 1996. MD simulations of Ag film growth using the Lennard-Jones potential. *Journal of Physics of Condensed Matter* 8:8753-8762.

Haile, J. 1997. *Molecular Dynamics Simulation: Elementary Methods*. New York: John Wiley & Sons Inc.

Hansen, J. and I. R. McDonald. 1986. *Theory of simple liquids*, Academic.

Happel, J. and H. Brenner. 1983. *Low Reynolds number hydrodynamics: with special applications to particulate media.* Hague, Netherlands: Martinus Nijhoff Publishers.

Humphrey, W., A. Dalke and K. Schulten. 1996. VMD - Visual Molecular Dynamics. *Journal of Molecular Graphics* 14: 33-38.

Koplik, J., J. Banavar and J. Willemsen. 1988. Molecular dynamics of Poiseuille flow and moving contact lines. *Physical Review Letters* 60: 1282-1285.

Koplik, J., J. Banavar and J. Willemsen. 1989. Molecular dynamics of fluid flow at solid surfaces. *Physics of Fluids* A: 1:781-794.

Koplik, J., M. Vergeles, P. Keblinski, and J. Banavar. 1996. Stokes drag and lubrication flows: A molecular dynamics study. *Physical Review E* 53:4852-4864.

Ohanian, H. 1995. *Modern Physics*. Englewood Cliffs, NJ: Prentice Hall.

Panton, R. 2005. *Incompressible flow*. New York: John Wiley & Sons Inc.

Rapaport, D. 2004. *The Art of Molecular Dynamics Simulation*. New York: Cambridge University Press.

Rapaport, D., Clementi, E. 1986. Eddy Formation in Obstructed Fluid Flow: A Molecular-Dynamics Study. *Physics Review Letters* 57:695-698.

Plimpton, S. 1995. Fast Parallel Algorithms for Short-Range Molecular Dynamics. *Journal of Computational Physics* 117: 1-19.

Sandberg, W., J. Waltz, O. Soto, R. Lohner and A. Shostko. 2002. Flows past single and multiple micro-spheres in micro-devices, *Fifth World Congress on Computational Mechanics*. July 2002, Vienna, Austria.

Stillinger, F. and A. Rahman. 1974. Improved Simulation of Liquid Water by Molecular Dynamics. *Journal of Chemical Physics* 60: 1545-1557.

Stokes, G. 1851. On the effect of the internal friction of fluids on the motion of a pendulum. *Proc. Cambridge Philos. Soc.* 9: 8-106.

Sun, M. and C. Ebner. 1992. Molecular dynamics study of flow at a fluid-wall interface. *Physical Review Letters* 69: 3491-3494.

Tehver, Riina, Flavio Toigo, J. Koplik and J. Banavar. 1998. Thermal walls in computer simulations. *Physical Review E* 57:R17-R20.

Travis, K. and D. Evans. 1997. Molecular spin in a fluid undergoing Poiseuille flow. *Physical Review E* 55: 1566-1572.

Travis, Karl P., B. D. Todd and Denis J. Evans. 1997. Departure from Navier-Stokes hydrodynamics in confined liquids. *Physical Review* E 55:4288-4295.

Verlet, L. 1967. Computer "Experiments" on Classical Fluids. I. Thermodynamical Properties of Lennard-Jones Molecules. *Physical Review* 159:98-103.

Veytsman, B. and M. Kotelyanskii. 1997. Periodic Boundaries for Off-Lattice Simulations. Potential cut-off. Penn State Polymer Physics Group. http://www.plmsc.psu.edu/~www/matsc597c-1997/simulations/Lecture3/node2.html (accessed February 26, 2006).

Zahn, D. 2004. How does water Boil? *Physical Review Letters* 93: 227801-4.

Ziarani, A. and A. Mohamad. 2005. A molecular dynamics study of perturbed Poiseuille flow in a nanochannel. *Microfluid Nanofluid* 2:12-20.

Vita

Vita of Tim Sirk

The author was born to Louie and Kay Sirk on July 27, 1980, in Gassaway, WV. He was raised near Charlotte, North Carolina where he attended the York County public school system. The author became an engineering student in 1998 at West Virginia University. As an undergraduate, the author researched hydrogen-fueled IC engines and developed an interest in fluid dynamics. He graduated from West Virginia University Institute of Technology with a Bachelor of Science degree in Mechanical Engineering in 2003 and began his pursuit of graduate study at Virginia Tech in 2004.